PB204809

AGE

1. Report No.	2. Government Accession No.	3. Recipient's Catalog No.
DOT-TSC-NHTSA-71-4		

4. Title and Subtitle	5. Report Date
Occupant Motion Sensors: Methods of Detection and Analysis	July 1971
	6. Performing Organization Code: TIF
7. Author(s): J. L. Horner, D.S. Ofsevit, G.R. Plank, G. G. Lawrence	8. Performing Organization Report No.
9. Performing Organization Name and Address: Transportation Systems Center, 55 Broadway, Cambridge, Mass. 02142	10. Work Unit No.: R1057
	11. Contract or Grant No.: 71-HS-05
12. Sponsoring Agency Name and Address: National Highway Traffic Safety Administration, Washington, D.C. 20591	13. Type of Report and Period Covered: Technical Report
	14. Sponsoring Agency Code

15. Supplementary Notes

16. Abstract

A study has been made of methods for measuring occupant motion within a vehicle during crash or impact conditions. The purpose of the measurements is to evaluate restraint systems, using anthropometric dummy, animal, or human occupants.

A list of general specifications for occupant motion sensors was drawn up. This was used to establish criteria for evaluation of proposed systems. From a study of various possible systems, five were selected for further development. These systems were built and prepared for field testing. In addition, computer methods for Fourier analysis of the data produced by these systems have been developed in theory and in programs for a digital computer.

17. Key Words	18. Distribution Statement
Bandwidth, Acceleration, Rotational Motion, Angular Motion, Fourier Analysis, Digital, Sensor, Filtering, Transducer	Unclassified - Unlimited

19. Security Classif. (of this report)	20. Security Classif. (of this page)	21. No. of Pages	22. Price
Unclassified	Unclassified	55	

Form DOT F 1700.7 (8-69)

TABLE OF CONTENTS

LIST OF ILLUSTRATIONS

LIST OF TABLES

1. 0 INTRODUCTION

During FY71 there were two phases to the Occupant Motion Sensors project: analysis and trade-off studies of possible systems, and development and testing of prototype systems. Since the first phase has been reported in detail it will only be summarized in this report, which will concentrate on the second phase.

The project started with the establishment of a list of general specifications for occupant motion sensors by TSC and NHTSA personnel. This list defined the measurements to be made, with the co-ordinate system, maximum expected value, priority, and accuracy of each measurement. See Appendix A.

The general specifications were used to calculate the performance requirements for candidate sensor systems. These requirements were used, along with additional considerations unique to measurement of occupant motions in a crash environment, to evaluate each proposed sensor system. This evaluation yielded five potentially useful systems. The process of evaluation is summarized in Section 2.0, and each of the five chosen systems is described in detail in Section 3.0.

A parallel study was made of methods for processing the data recorded from a sensor, resulting in several new digital filtering techniques which were tested on a Honeywell DDP-516 computer. The results of this study are described in Section 4.0.

2.0 ANALYSIS AND TRADE-OFF STUDIES

The most obvious performance requirements for an occupant motion sensor are those stated directly in the general specifications, i.e., the peak expected value and the relative priority of each quantity. Two other important requirements, the bandwidth and mass of a sensor, were computed from the general specifications.

Bandwidth, which is given in units of frequency, is a measure of the speed of a device. If a system has a wider bandwidth than another, it can respond more quickly to inputs. In an electro-mechanical system, the input is the motion of the device and the output is an electrical signal which contains information about that motion. Most standard electro-mechanical sensors have bandwidths on the order of 100 Hz or less. To determine the required bandwidth for occupant motion sensors, a mathematical model was made of a crash deceleration using the maximum specified values for position, velocity, and acceleration. Fourier analysis of the model (5, pp. 6-14) gave the minimum bandwidths which various sensors must have to meet the 5% accuracy requirement. See Table 1. In all cases, the bandwidths are wide enough to preclude the use of nearly all standard electro-mechanical sensors.

TABLE 1. - REQUIRED SENSOR BANDWIDTH

Quantity Measured	Bandwidth for 5% Error (Hz)
Acceleration	425
Velocity	380
Position	665

The mass of an occupant motion sensor must be small enough so that it does not have too large an effect on the motion which it measures. The most sensitive case is head motion, since the head is lighter than the torso and undergoes more violent motion. Using the general specifications for maximum angular velocity and acceleration of the head, it can be shown*(5, pp. 50-51) that a 1/2-ounce (14-gram) sensor can exert up to 11 pounds of force on its mounting device. This maximum mass also precludes the use of most standard electro-mechanical sensors. See Appendix B for mounting requirements imposed by sensor mass.

*Note a misprint on p. 51 of the reference, which should read 12.6 ounces, not 12.6 pounds.

The general specifications stress the importance of the measurement of rotational motion. A growing body of evidence indicates that rotational, not linear, motions of the head-torso system are mainly responsible for injuries to this region of the body. Instrumentation currently in use at major sled and car crash test facilities is limited to high-speed cameras and linear accelerometers. Of the latter, piezoresistive, piezoelectric, and strain gauge are the most popular types. Rotational motion is difficult to measure with such equipment. To convert linear acceleration to rotational acceleration, a center of rotation must be defined. In a mechanical system as complicated as the head-neck-torso system, the center of rotation is not well-defined, as it changes with time. High-speed film, in its present form, does not yield accurate quantitative data. Each frame must be examined for incremental motion by a human operator. This procedure is tedious, time-consuming, and error-prone. Also, it yields positional data and must be differentiated, once to yield velocity and twice to yield acceleration. In Section 4.1, it is shown that any error which is present in the positional data will increase by 40% each time the data is differentiated. For these reasons it was anticipated that, while available equipment might be useful for measuring linear motion, new systems would have to be developed to measure rotational motion.

Table 2 contains a complete list of all occupant motion sensor systems that were evaluated. In addition to the requirements discussed above, a list of twelve other criteria for sensors was assembled (5, pp. 14-17). See Table 3. The maximum score for each category shows the relative importance assigned to that category. Crash survivability alone could reject a system; indeed it eliminated several exotic ideas which would have required delicate sensors on board the test sled or vehicle. The total score from this list, along with the requirements discussed above, was used to decide whether a system should be developed (5, pp. 18-38). Information needed to make these ratings and decisions came from many sources: discussions with people in the field of deceleration sled testing, a survey of the open literature, a survey of manufacturers, discussions with manufacturers and their technical engineering personnel, and calculations of probable performance.

TABLE 2. - CANDIDATE SENSOR SYSTEMS

A. Mechanical

1. Gyro
2. RVDTA
3. Potentiometers
4. Strain Gauge
5. Linear Velocity Transducer
6. Accelerometer

B. Optical

1. High Speed Photography
2. Laser Doppler System
3. Laser Range Finder
4. Holography
5. Ellipsometry

C. Electromagnetic, High Frequency

1. Doppler Radar
2. FM Phase Lock

D. Ultrasonic or Acoustic

1. Doppler Shift
2. FM Phase Lock
3. Signal Strength
4. Interferometry

E. Electromagnetic, Low Frequency

1. Capacitance Variations
2. Magnetometer
3. Radio Direction Finder

TABLE 3. - CRITERIA LIST

		Weight
1.	Crash Survivability	+,-
2.	Accuracy & Calibration Stability	15
3.	Freedom from Spurious Outputs	15
4.	Unique Advantages or Disadvantages	10
5.	Data Reduction Requirements	10
6.	Reliability	10
7.	Development Costs	9
8.	Maintenance Required	9
9.	Signal/Noise Ratio	8
10.	Level of Personnel Required to Operate System	6
11.	Measurement Taken	5
12.	Power Requirements	3
		±100

3.0 CANDIDATE SYSTEMS

Five sensor systems in Table 2 passed the process of evaluation described in Section 2.0. The development of each is described below. Some problems have already been found which were not anticipated during system evaluation, and more may arise during field testing. This section discusses the details and present status of each system.

3.1 POTENTIOMETER

In this sensor a variable resistor is controlled by linear motion. The equivalent circuit is shown in Figure 1. It is suitable for measuring linear displacement only and would thus be limited to torso measurements. The bandwidth of this type of device is limited only by distributed capacitance in the resistive windings; this is usually quite small, and a typical bandwidth is 100 kHz.

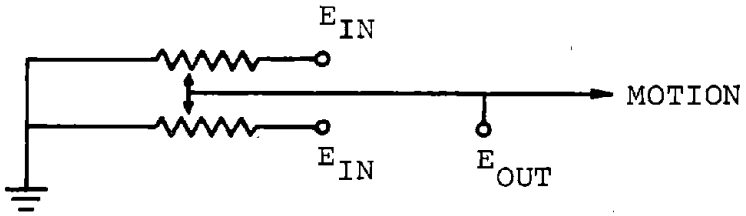

Figure 1. - Schematic Potentiometer System

Two versions of the potentiometer have been considered. The first would use a rectilinear potentiometer, with the movable contact connected to a straight rigid bar. To follow the motion of the subject, the device would have to be mounted on a gimbaled mount (Figure 2). This arrangement is quite bulky and, because of the rigid connection to the subject, apparently too dangerous for use with human subjects.

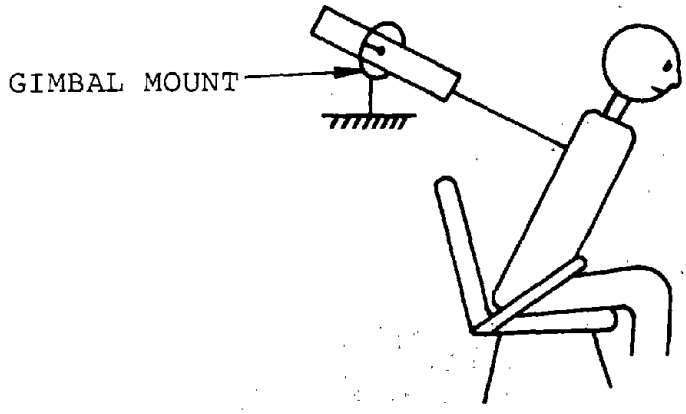

Figure 2. - Mounting of Rectilinear Potentiometer

The second version of this idea uses a rotary potentiometer whose shaft is wound with a flexible cable. A rigid connection is not needed because a spring motor attached to the shaft keeps the cable taut. The attachment of the cable to the shaft converts linear motion to rotary motion. A commercially available device of this type* is shown in Figure 3. This unit is compact and sturdy enough for mounting on the test sled or vehicle. The flexible cable eliminates the safety hazard discussed above. The present unit can not follow motion at the maximum acceleration (100 g) in the general specifications, but the principle is good and a more refined version can probably be built. We will therefore include this unit in field tests.

Since the motion is measured along the direction of the cable or rigid bar, vector error will be present in both versions. As the angle between this line and the torso departs from 90 degrees, the measured motion includes components which we do not desire. However, since we know the approximate torso orientation where maximum motion occurs, the mounting of the sensor can be preset to minimize such error components.

*Houston Scientific Inc., 4202 Directors Row, Houston, Texas, 77018.

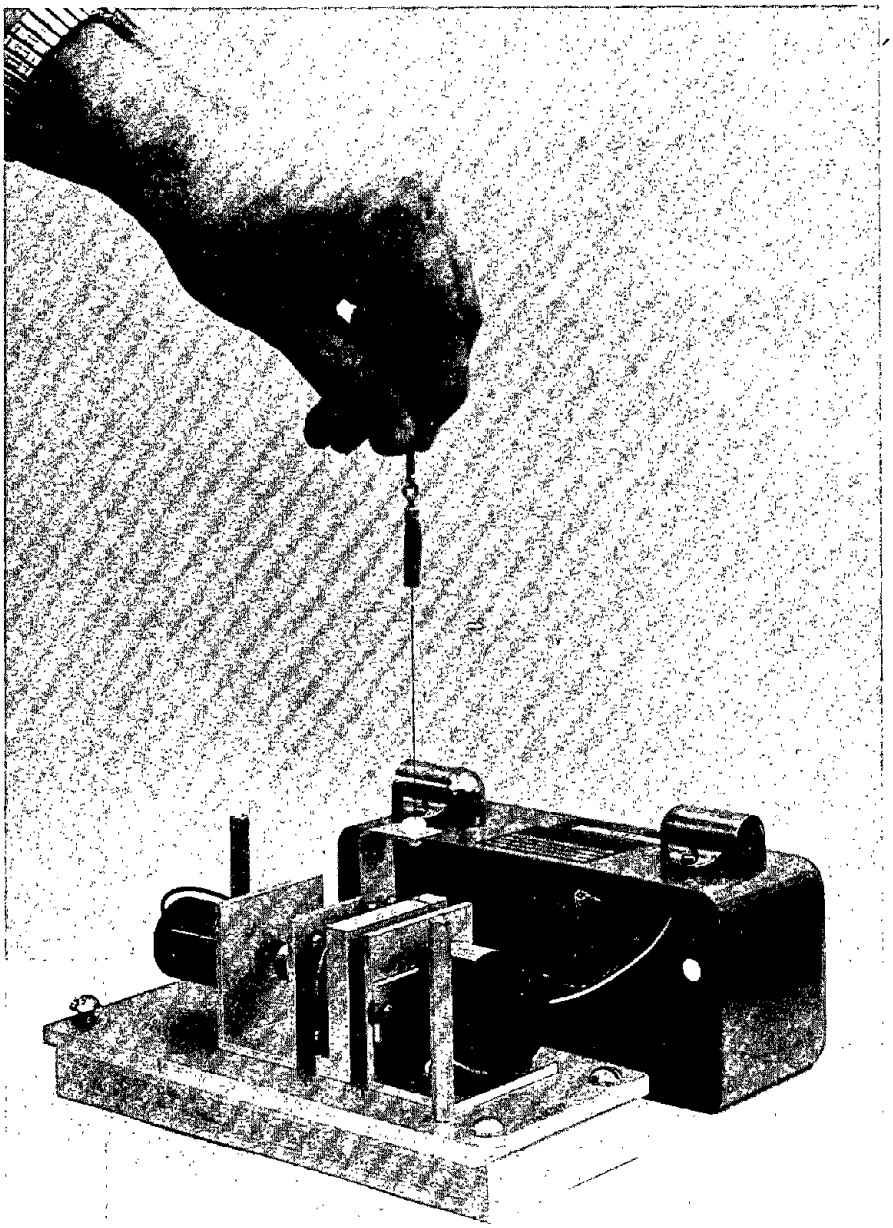

Figure 3. Rotary Potentiometer

3.2 LINEAR VELOCITY TRANSDUCER

There are two possible versions of this sensor. The first is attached to the rotary potentiometer discussed in Section 3.1. A tachometer attached to the same shaft gives a velocity output signal. Since the unit was purchased primarily because of the potentiometer, no preliminary work was done on the tachometer. Therefore, it has not yet been tested.

Another version is mechanically similar to the rectilinear potentiometer, and has the same mounting and safety problems. In it, a permanent magnet moves through a long coil and gives a voltage output proportional to velocity. The bandwidth is limited by the internal resistance of the coil. In a commercially available unit* the bandwidth was calculated to be 68 kHz, not taking into account capicitance between turns of the coil. It is anticipated that the bandwidth will still be considerably greater than the minimum requirements, even when the inter-turn capacitance is included.

3.3 ELLIPSOMETRY

This concept attempts to overcome the two main problems of high-speed photography: extraction of accurate data and measurement of rotational motion.

The system is illustrated schematically in Figure 4. A high-speed, on-board camera records a small lightweight target taped to the head; (High-speed cameras are available which can withstand the shock of a crash test). On-board mounting makes it possible to record motion with respect to the test vehicle, which is desirable. The target (Figure 5) consists of a circle and sphere aligned coaxially.

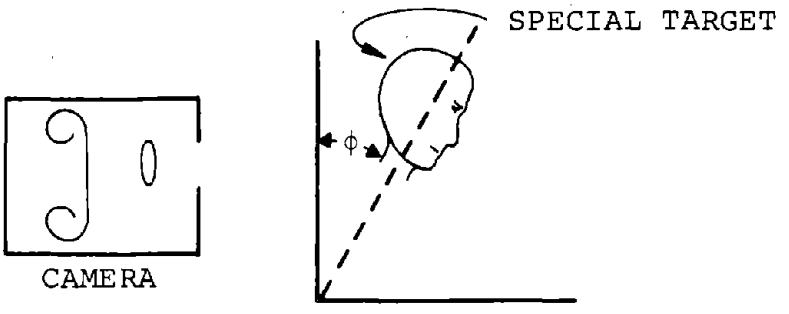

Figure 4. - Schematic Illustration of Ellipsometry

*Hewlett-Packard Corp, Palo Alto, Calif. No. 7LV20.

Ratio of Axes: $\frac{R \cos \phi}{R} = \cos \phi$

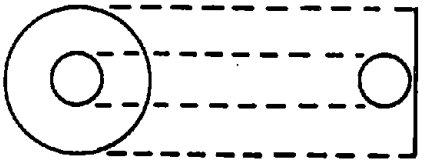

Figure 5. - Ellipsometry Target

As the head rotates forward in Figure 4, the camera sees the circular part of the target become elliptical. The eccentricity, ε, is related to the angle of tilt, ϕ, as:

$$\varepsilon = \cos\phi \qquad (1)$$

The spherical part of the target, colored to make it distinct from the circular part, appears to become smaller as it moves away from the camera. This makes it possible to extract linear motion from total motion.

An important source of error in conventional semi-automatic film scanners is the need for an operator to line up a set of cross-hairs on a selected fiducial point on each frame of film. This would be avoided here by using a computer-based opto-electronic system developed by TSC. This system is part of the remote occulometer, or eye motion tracking system, and automatically detects and measures the eccentricity of a high-contrast disc. The computer could also be used to correct displacement errors caused by the high-speed camera's optical system, once the camera has been calibrated.

The target could easily meet the maximum mass requirement in Section 2.0. It would have to be about one inch in diameter to keep measurement error below 5%. Since it could consist of simple diffusely reflecting material, its weight could be kept below 10 grams.

A working model of this system has not been developed. New equipment would have to be procured to allow the occulometer

to scan photographic film. This has not been done because of the promise of other sensors whose output can be read more directly, particularly the angular position detector discussed in Section 3.5.

3.4 ROTATIONAL ACCELEROMETER

The interim report (5, Appendix C) contains a proof that two linear accelerometers, properly aligned, can detect rotational acceleration. For the array in Figure 6, the relation is:

$$\ddot{\phi} = \frac{A_{a\perp} - A_{b\perp}}{d} \qquad (2)$$

The accelerometers are internally wired to perform this calculation so that the resultant output gives angular acceleration directly. A manufacturer* was found to supply two prototype models.

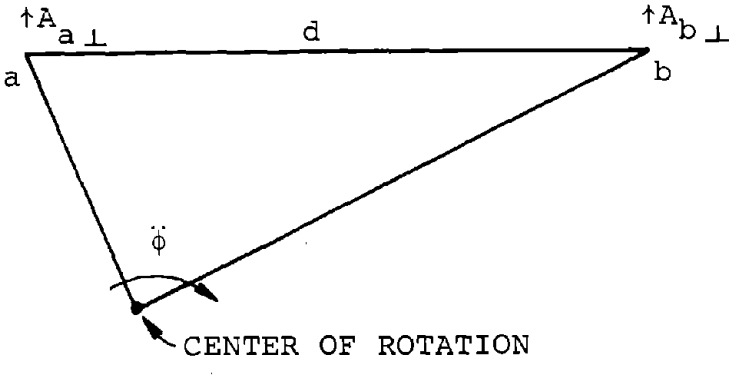

Figure 6. - Rotational Acceleration from Two Linear Accelerations

Although this arrangement should theoretically be sensitive to rotational acceleration only, there are two possible sources of error. The subtraction in equation (2) should remove the linear acceleration common to both terms. If the two linear accelerometers do not have exactly the same sensitivity, there will be a net linear term. The manufacturer specifies this imbalance as 1%. The other source of error

*Columbia Research Laboratories, Woodlyn, Pa.

arises from the sensitivity of each accelerometer to motion along axes other than the specified axis. This is also less than 1% in the supplied units. Therefore, with these major sources contributing less than 2% error, this method meets the specification for accuracy.

Laboratory calibration of the rotational accelerometers was conducted using a shake table driven in simple harmonic motion. Attached to the shake table was a fixture which converted the linear motion of the table into angular motion. The accelerometer was attached to this fixture. See Figure 7. The amplitude of the motion of the accelerometer was observed through a stereoscopic microscope. Since the shake table was driven at the frequency ν, this gave a rotational motion (in complex notation) of:

$$\phi = R\frac{X_o}{2} e^{i2\pi\nu t} \text{ rad} \qquad (3)$$

X_o is the observed amplitude; R the radius of rotation measured on the test fixture. Differentiating twice, we get angular acceleration:

$$\ddot{\phi} = -R\frac{X_o}{2}(2\pi\nu)^2 e^{i2\pi\nu t} \text{ rad/sec}^2 \qquad (4)$$

The amplitude E_o of the voltage output of the transducer was measured on a meter, so that the voltage could be expressed as:

$$E = E_o e^{i2\pi\nu t} \text{ volts} \qquad (5)$$

The calibration of the accelerometer was then:

$$\frac{|E|}{|\ddot{\phi}|} = \frac{E_o}{R\frac{X_o}{2}(2\pi\nu)^2} \text{ volts/rad/sec}^2 \qquad (6)$$

For the supplied accelerometers, sensitivity was 8.1×10^{-6} volts/rad/sec^2, with a measured standard deviation of 3.7% over a range of frequencies.

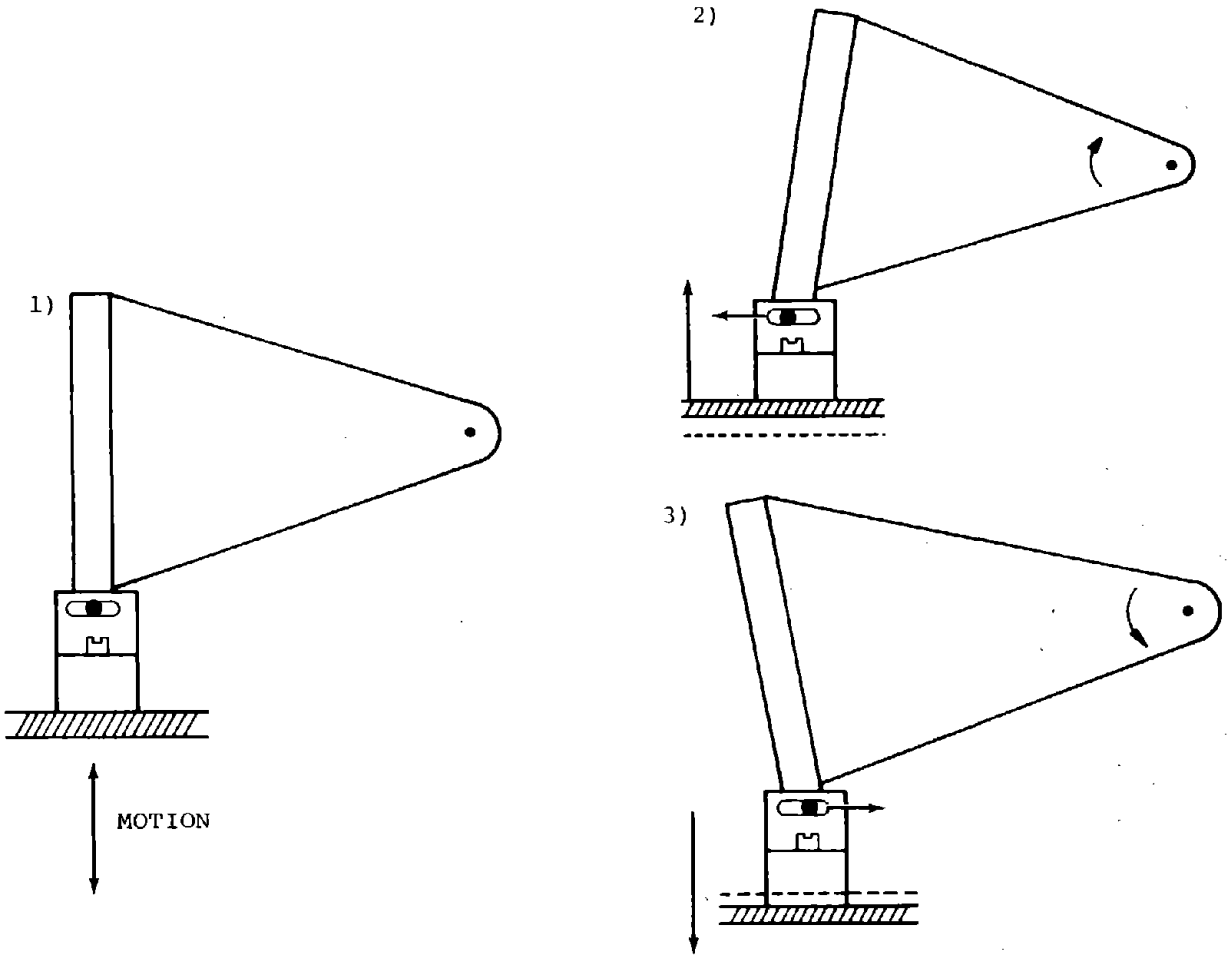

Figure 7. - Schematic of Conversion from Linear to Rotational Motion

1. Fixture on Shake Table at Rest
2. Fixture Converts the Linear Upward Motion of Table to Rotational Motion
3. Fixture Converts Linear Downward Motion to Rotational Motion

To measure sensitivity to linear motion caused by differences between the two linear accelerometers in a unit, the rotational accelerometer was subjected to linear motion on the shake table. The imbalance was measured as 1.5%; i.e., the output was 1.5% of the manufacturer's specified output for each separate linear accelerometer. This value was close to the 1% discussed above.

Because of limitations in visually observing the motion of the shake table, these calibrations have been limited to frequencies below 100Hz. When a calibrated linear accelerometer with wide bandwidth is available, it will be used to measure the motion of the shake table so that calibration of the rotational accelerometer up to at least 1 kHz can be accomplished.

The rotational accelerometer as supplied meets the requirements for sensor mass. It is somewhat too large to mount on a bite bar (see Appendix B), but this problem can probably be overcome with further development.

3.5 ANGULAR POSITION DETECTOR*

The Angular Position Detector (APD) measures the angle between a small radio frequency (RF) coil and a spatially uniform RF magnetic field. The system originally proposed would have used a pair of Helmholtz transmitting coils to create the magnetic field (Figure 8). The voltage output of each sensor coil would be proportional to the sine of the angle between its axis and the direction of the field. These sensor coils would be mounted on the vehicle occupant.

This configuration was analyzed to determine its feasibility. Section 3.5.1 shows that prohibitively large coils would have been needed to create a uniform field large enough to measure occupant motion with 5% accuracy. Section 3.5.2 describes the development of a single smaller coil located at a relatively large distance from the sensor. This system is shown in Figure 9.

*An invention disclosure of this system has been filed with the TSC Patent Attorney.

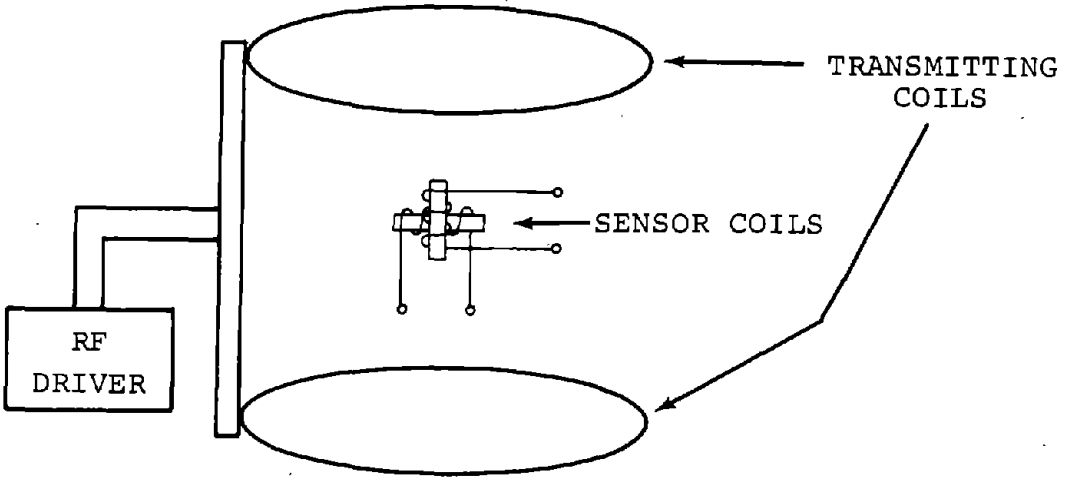

Figure 8. - Original Proposed APD System

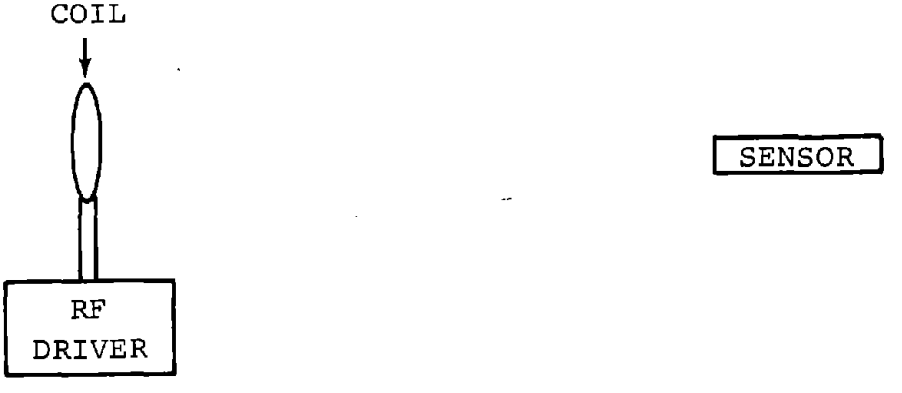

Figure 9. - Final APD System

The RF transmitter coil operates at a frequency of 50 kHz. This frequency represents a compromise between conflicting requirements. To minimize distortion of the field by metal members of the test sled, rails, dummy's body, etc., the frequency should be kept low. Such metal members act as conductors and can distort a magnetic field. At lower frequencies the wavelength of the field becomes longer, and conductors become less efficient. On the other hand, a higher frequency improves the efficiency of the pickup coil and allows for wider electrical bandwidth.

The output of the sensor is a 50 kHz carrier signal, amplitude modulated by a signal (12, pp. 36-37) proportional to the angular motion of the sensor coil. Section 3.5.4 discusses the electronics needed to amplify and detect this signal. These electronics were developed in a small enough package to be mounted on the test vehicle. Section 3.5.5 discusses preliminary static tests of the system.

3.5.1 Analysis of Helmholtz Coil Configuration

The magnetic flux vector at a point P (Figure 10) for a single turn of wire is:

$$\underline{B} = \frac{\mu I}{4\pi}\left[\underline{i}\int_0^{2\pi}\frac{RZ\sin\phi}{(r^2-2rR\cos\phi+R^2+Z^2)^{3/2}}\,d\phi + \underline{j}\int_0^{2\pi}\frac{RZ\cos\phi}{(r^2-2rR\cos\phi+R^2+Z^2)^{3/2}}\,d\phi + \underline{k}\int_0^{2\pi}\frac{R(R-r\cos\phi)}{(r^2-2rR\cos\phi+R^2+Z^2)^{3/2}}\,d\phi\right] \qquad (7)$$

μ is the permeability of the medium, I the current in the coil. These integrals were calculated using Simpson's Rule on a programmable calculator.*

*Hewlett-Packard 9100A, Program No. 70015

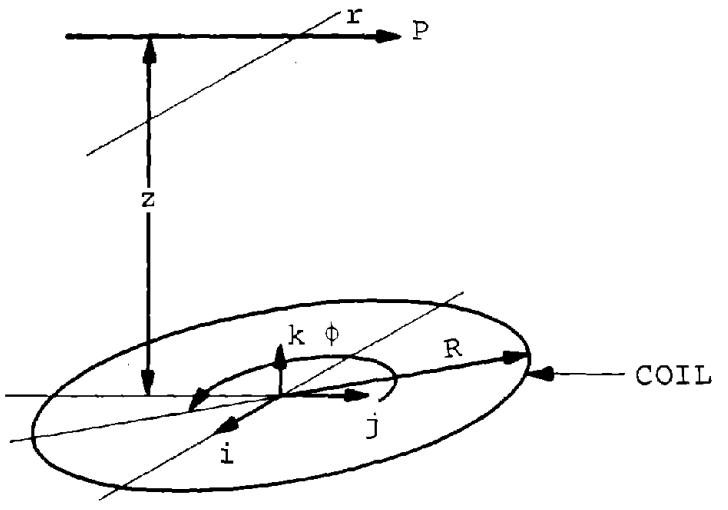

Figure 10. - Co-ordinate System for a Coil

The field produced by a Helmholtz coil pair was then calculated. To have no error, we would require that the field be everywhere parallel to the axis of the coils. For a Helmholtz coil pair, the angle between the field and the axis increases, in general, with the distance from the axis. When this angle would be 90°, there would be 100% error; therefore to have 5% error we would need to have our occupant motion confined to the region where the angle would be less than 4.5°. From the general specifications we know that this region is approximately one cubic meter. Contours of field angle deviation from axis were calculated for several Helmholtz coil configurations; an example is shown in Figure 11. Since the occupant motion must be contained within the 5°-deviation lines, the coil radius would have to be several meters, which would be much too large to be used in actual field tests.

3.5.2 APD Transmitting Coil

In the case where the Helmholtz coils are small compared to the distance between them, it was found that the angular deviation problem described above is improved. This improvement suggested the use of a single coil whose size is small compared to its distance from the sensor. At a distance of 20 meters, the field angle stays within 5% of the axial direction up to 1 meter off the axis.

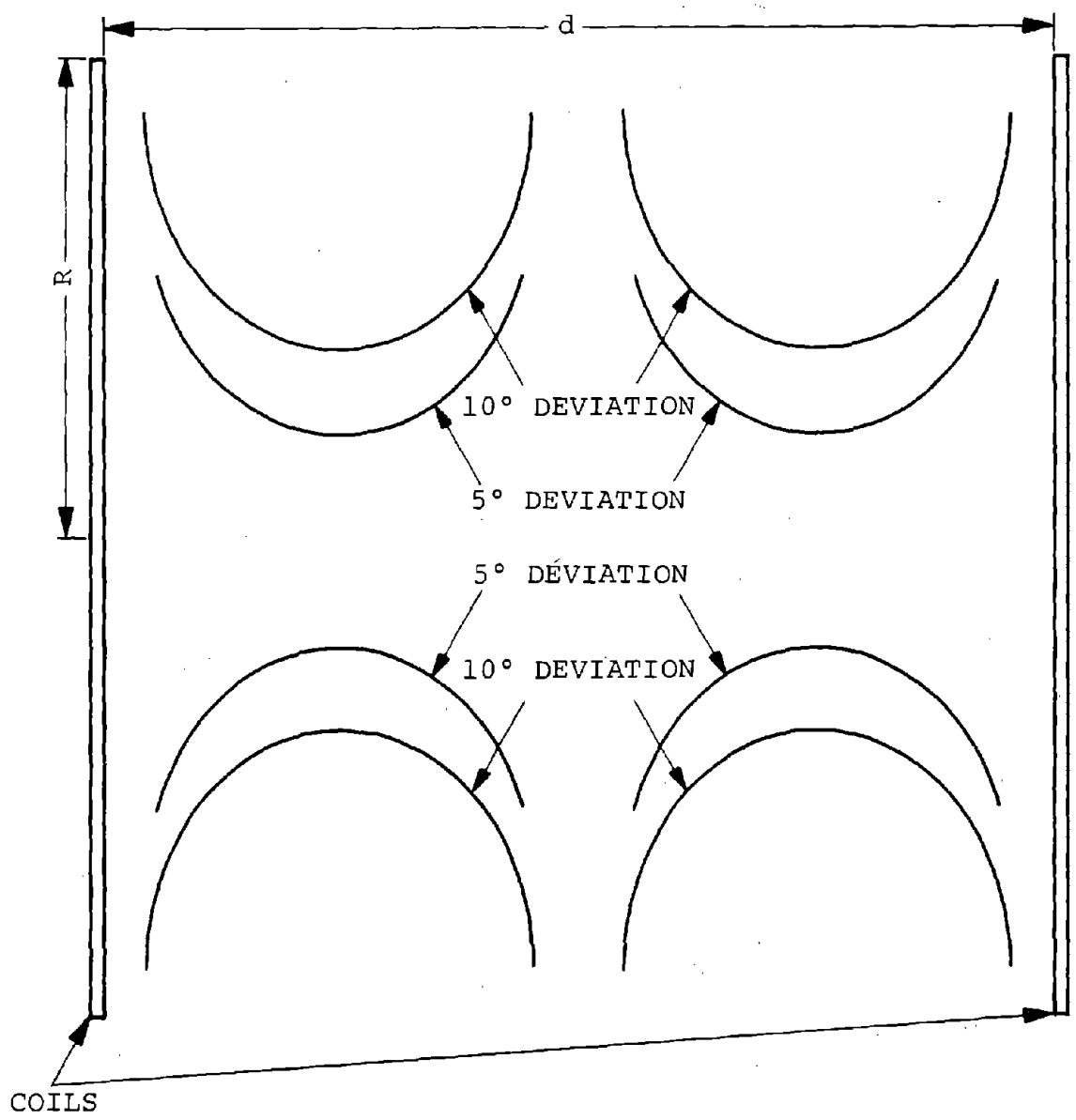

Figure 11. - Lines of Constant Magnetic Field Angle for Helmholtz Coil Pair; Ratio d/R = 2

A series resonant circuit (Figure 12) was selected to obtain maximum current in the coil and hence maximum field strength. The coil was wound, using #22 wire, on a circular wooden form, 6" in diameter. It was found that 117 turns of wire made the tuned circuit (capacitor and coil) match the 16 Ω tap on the amplifier; this length of wire does not have that much resistance, so other losses in the circuit have a great effect on its impedance. The coil voltage that could be achieved with this configuration was at least 6000 volts peak-to-peak, which was more than adequate for initial APD tests. Further improvements on the coil are anticipated.

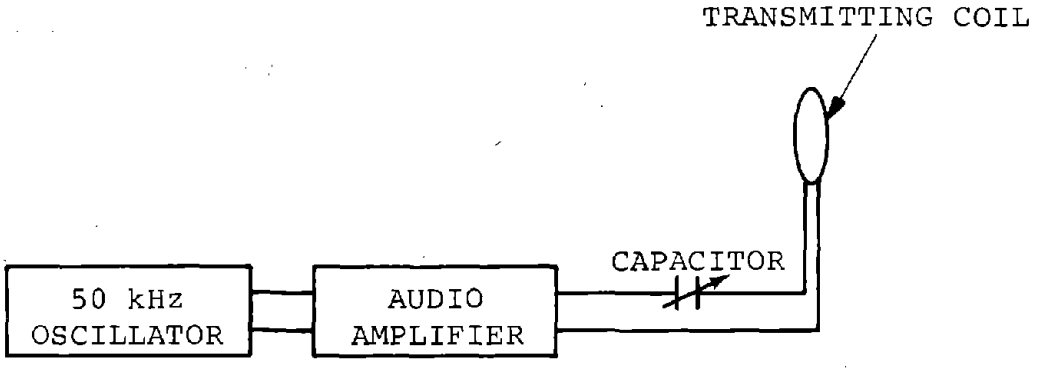

Figure 12. - Transmitting Coil Circuit

3.5.3. APD Sensor

The sensor consists of a ferrite core RF choke coil in parallel with a silver mica capacitor. Their present values are 2200 μh and 4300 pf respectively. These components have been cast firmly in place in a small plexiglass box, less than 1" long.

The peak frequency response of the sensor has been measured at 50.1 kHz. The 1 dB bandwidth is 1 kHz, while the 3 dB bandwidth is 3 kHz. This bandwidth could be broadened by adding a resistor to the sensor circuit.

3.5.4 APD Receiver

Figure 13 shows the complete circuit of the APD receiver used in preliminary static tests.

Since the sensor has high impedance, the input stage of the receiver must have very high impedance. When the sensor is 30' from the transmitting coil, its maximum peak-to-peak voltage is approximately .5 mv. To have a 5 v peak-to-peak output, the receiver must have a gain of 10,000 (+80dB).

A Fairchild #739 integrated circuit contains two identical operational amplifiers. It was chosen for use here because of its high input impedance, high gain-bandwidth product, and low noise. The first stage of the receiver uses one of the operational amplifiers in a non-inverting mode. This stage is designed for a gain of 220 and uses a series RC circuit at its negative input to limit low-frequency response. The second stage of the receiver uses the other operational amplifier, this time in inverting mode. This stage has a gain of 50 and uses a series RC circuit at the positive input, again to limit low-frequency response. In both stages high-frequency response is limited by the internal characteristics of the operational amplifiers. Capacitive coupling is used between these stages and between the second stage and detector as well. This eliminates the need for trim potentiometers to adjust d.c. offsets.

The theoretical gain of the two amplifier stages should thus be 11,000. Figure 14 shows the measured response, with a peak gain of 10,000 at a center frequency of 50 kHz. The 1 dB bandwidth is 13.5 kHz, while the 3 dB bandwidth is 28 kHz.

Because of the capacitive coupling, a simple diode detector could not be used. The coupling capacitor in series with a diode would act as a clamping circuit, and no signal could get through. Therefore, a resistance was placed before the diode to give the coupling capacitor a discharge path to ground. A resistive divider was added to bias the diode at 0.2 volts so that it can pass a very small signal. The detector circuit has a bandwidth of about 1 kHz, which is wide enough to meet the system bandwidth requirement.

The output stage uses a Philbrick #1021 operational amplifier with unity gain. This re-inverts the signal and gives the receiver low output impedance so that it can feed the long cable to the recorder. The maximum output of the receiver circuit is about 2.5 volts d.c. at a coil-to-sensor distance of 30'. The signal-to-carrier ratio is 40 dB.

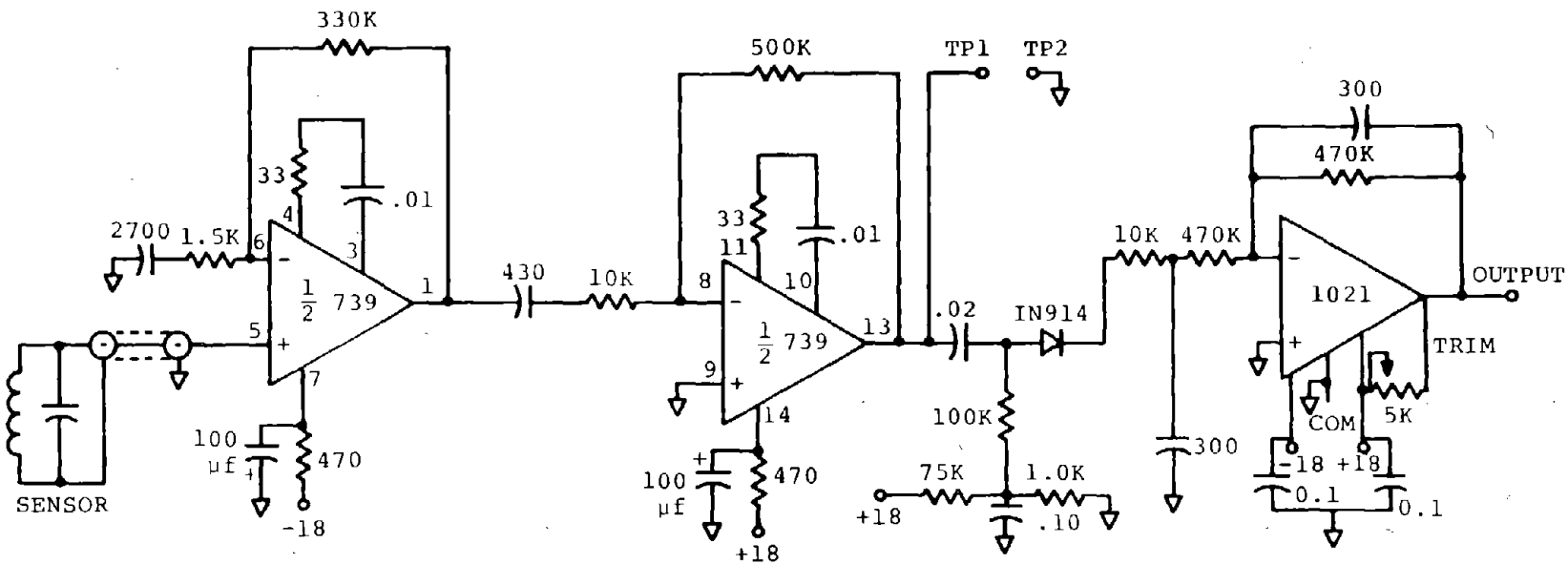

NOTES:

All resistors 5% tolerance
All capacitors 5% silver mica except .01 and .02 (ceramic)
Entire unit to be placed in a shielded minibox

Figure 13. - APD Amplifier and Detector Circuit

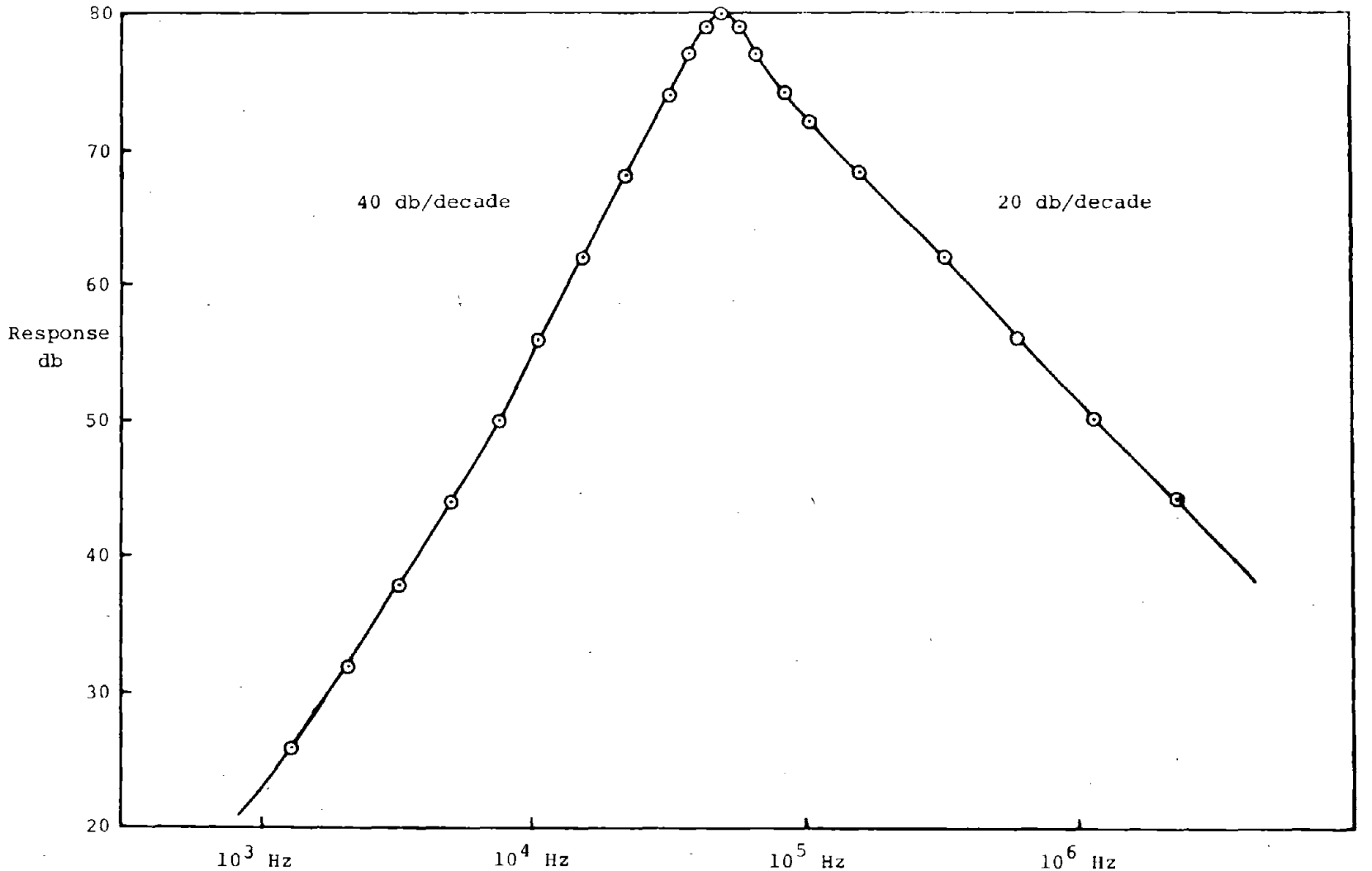

Figure 14. APD Amplifier Response

3.5.5 Static APD Tests

Static testing of the APD was performed at the Liberty Mutual Research Center, Hopkinton, Mass., which has a deceleration sled and standard Sierra test dummies. The sensor was first calibrated using the device shown in Figure 15. Readings of output voltage vs. angular position were taken with the transmitting coil 28', 29', and 30' from the sensor. Figure 16 shows a typical curve. In all cases the results were within 1.5% of the expected sine curve.

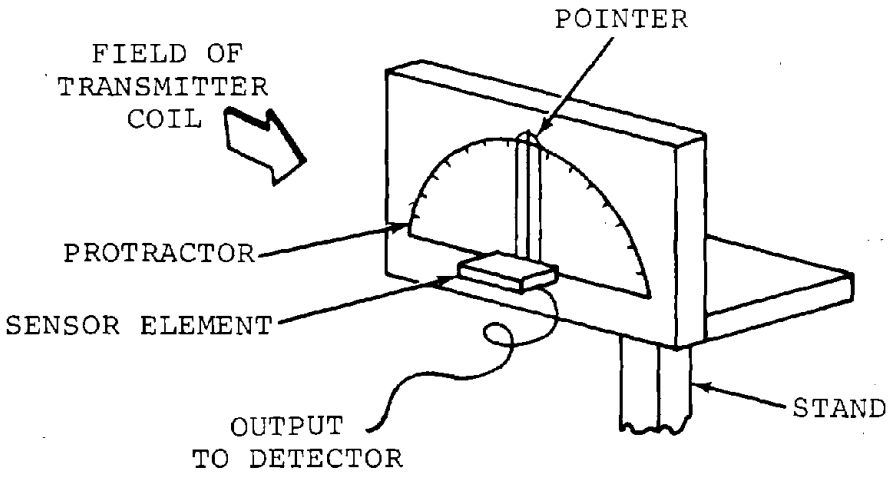

Figure 15. - APD Calibration Device

The APD was then tested to determine the effect of the dummy's aluminum frame on the system. The sensor was attached to the dummy's head, along with a quadrant black and white target. The dummy was moved in small increments to various angular positions. At each position the APD voltage was read and a photograph of the dummy was taken. The head angle corresponding to each APD reading was later measured from the proper photograph. Figure 17 shows the results. Some of the apparent error may have been caused by inaccuracies in measuring angles from photographs. In general, the data points agree closely with the data in Figure 16 and indicate that the dummy's frame, along with the metal superstructure of the test sled, will not cause significant problems with the APD.

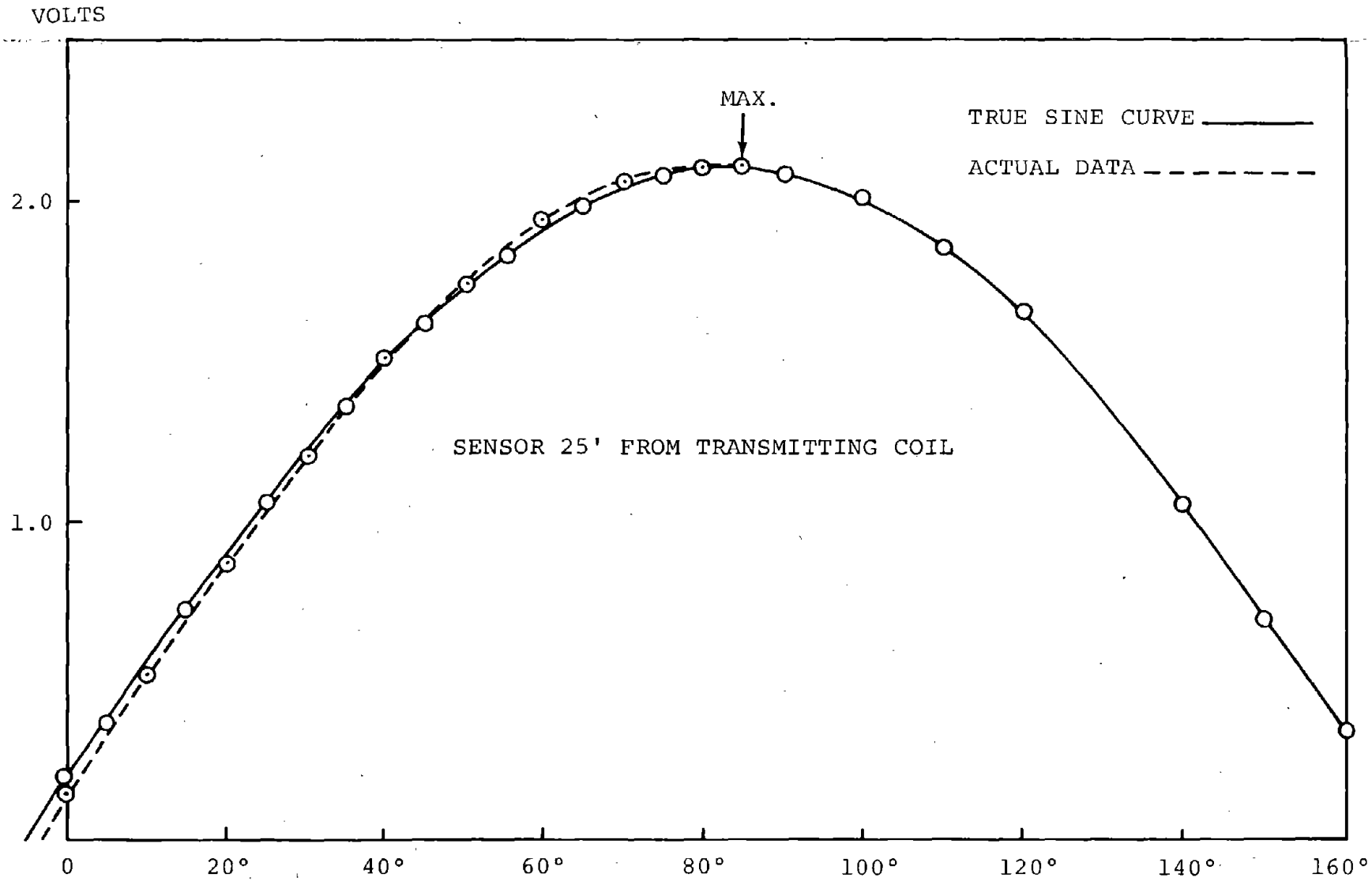

Figure 16. - Typical APD Calibration Curve

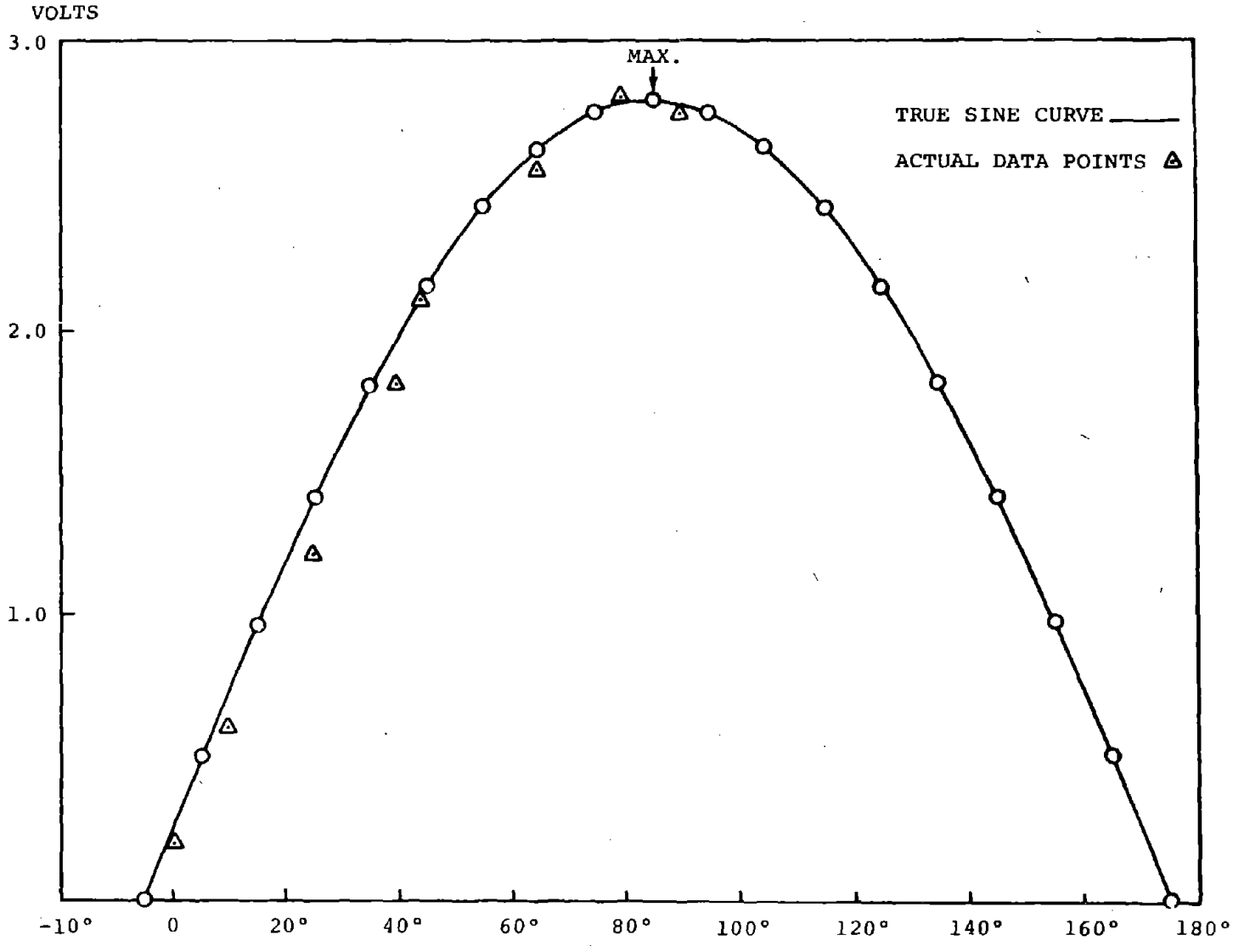

Figure 17. - Static APD Calibration, with Dummy

4.0 COMPUTER STUDIES

4.1 DIGITAL FILTERING

The raw signal produced by an occupant motion sensor during a test run is not usually useful without additional processing since the information may be buried under noise and artifacts. Noise comes from electrical transients and disturbances, vibrations and natural resonances in the complex mechanical systems involved, while artifacts are present because any sensor, no matter how well designed, will react (however slightly) to phenomena different from that which it is intended to measure.

The useful part of a signal can be obtained in a "brute-force" way by repeating the experiment many times and taking an average of the signals. However, time and expense usually require that we make more efficient use of the sensor signals from each test run. This is possible if we have some *a priori* knowledge of the system and what signal, noise, and artifacts we should reasonably expect. We can then apply more sophisticated methods of signal processing than mere averaging.

The signal produced by an occupant motion sensor is a function of time, recorded as pictures on film or as a voltage on magnetic tape. In this discussion, time functions will be referred to in the lower case: f(t). It is then natural to consider the use of Fourier Transform theory in processing f(t). Experience has proven the effectiveness of this method, and a great body of literature and practical experience exists. In addition, recent software advances have made it feasible to use the digital computer for Fourier analysis and synthesis, as will be discussed.

The general picture of a "filter" to process a signal is as follows:

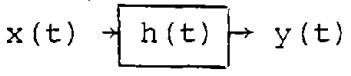

Figure 18. General block diagram of a filter

x(t) is the raw signal, say, the output of a sensor. It is fed into a black box, or filter, which reacts to x(t) in such a way as to produce y(t) at its output. h(t) is the impulse response of the filter y(t) = h(t) when x(t) is the impulse function $u_o(t)$:

$$u_o(t) = \begin{cases} 0, t \neq 0 \\ \text{undefined}, \ t = 0 \end{cases} \qquad (8)$$

and

$$\int_{-\infty}^{\infty} u_o(t)dt = 1 \qquad (9)$$

$u_o(t)$ is also known as the Dirac delta function, or simply the delta function. The theory of linear systems characterizes a

filter, as seen from its input and output, by h(t).(1,2)

The relationship of x(t), h(t), and y(t) is the mathematical relationship known as convolution, which is defined by the convolution integral:

$$y(t) = \int_{-\infty}^{\infty} x(\tau)h(t-\tau)d\tau \qquad (10)$$

Even with a computer, integration is a difficult and time-consuming operation which we wish to avoid.

Here the Fourier Transform enters. For a periodic time function, defined by:

$$f(t+T) = f(t) \quad \text{for all } t \qquad (11)$$

Fourier theory shows that we can express f(t) as a sum of fundamental and harmonic frequencies, done in complex number notation as:

$$f(t) = \sum_{-\infty}^{\infty} F_k e^{\frac{i2\pi kt}{T}}$$

where T is the period of f(t), $i = \sqrt{-1}$, and F_k are the so-called Fourier Coefficients. For a general time function, the discrete set of frequencies in the above series:

$$\nu = 0, \pm \frac{1}{T}, \pm \frac{2}{T}, \ldots \qquad (12)$$

for

$$k = 0, \pm 1, \pm 2, \ldots \qquad (13)$$

is not sufficient, since in general $f(t+\tau) \neq f(t)$.

For such a non-periodic signal we must consider all possible frequencies, changing the summation to its generalization, the integral:

$$f(t) = \int_{-\infty}^{\infty} F(\nu)e^{i2\pi\nu t}\, d\nu \qquad (14)$$

where F(ν) is now a function, known as the Fourier Transform or the spectrum of f(t). In this discussion functions of frequency will be referred to in the upper case: F(ν). The following can also be shown:

$$F(\nu) = \int_{-\infty}^{\infty} f(t)e^{-i2\pi\nu t}\, dt \qquad (15)$$

so that we can perform the transform in both directions. We write this fact as:

$$f(t) \leftrightarrow F(\nu) \qquad (16)$$

and call this a Fourier Transform Pair.

The usefulness of this theory for us is as follows. We can apply the Fourier Transform to each part of Figure 18:

$$x(t) \leftrightarrow X(\nu) \tag{17}$$

$$h(t) \leftrightarrow H(\nu) \tag{18}$$

$$y(t) \leftrightarrow Y(\nu) \tag{19}$$

Then by inserting the proper relations into the convolution integral, it can be shown that:

$$Y(\nu) = X(\nu)H(\nu) \tag{20}$$

In this relation, $H(\nu)$ is known as the transfer function of the filter. Now, if we had a way to calculate the Fourier Transforms in both directions, we would be able to replace the convolution integral by a multiplication of complex functions, which is in general a simpler operation. The system would then be:

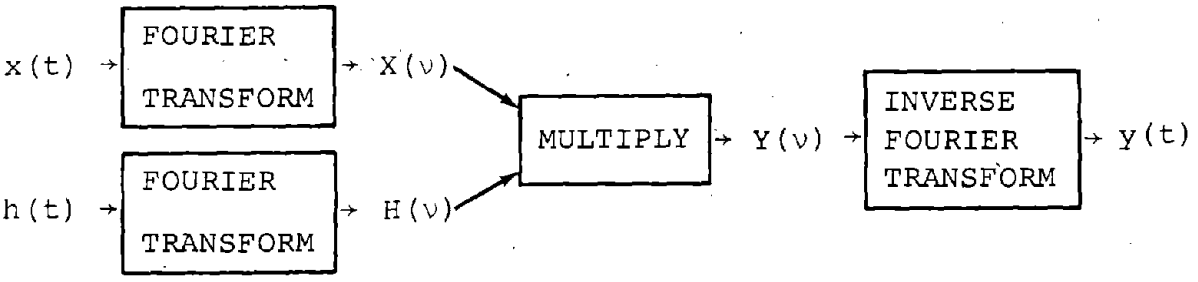

Figure 19. General Block Diagram of Filtering by Multiplication of Fourier Transforms

This theory has been known for many years, but for computation it long seemed no more practical than convolution, since computation of the Fourier Transform also requires the evaluation of an integral.

This difficulty has been overcome in the past few years through the use of a computer technique known as the Fast Fourier Transform (FFT), the most famous description of which is the paper by Cooley and Tukey in 1965.(3) A detailed derivation of the FFT will not be undertaken here. In general, it operates on the subscripts of a large array of numbers in order to replace complex multiplications (which are time-consuming computer operations) by complex additions (which are much faster). The book by Gold and Rader contains details and a bibliography. (4)

The chief limitation on the FFT is actually a limitation of the digital computer: finite memory. The core memory of the computer can not contain data about the infinite number of data points in a real time function. It is necessary to consider only a finite time interval:

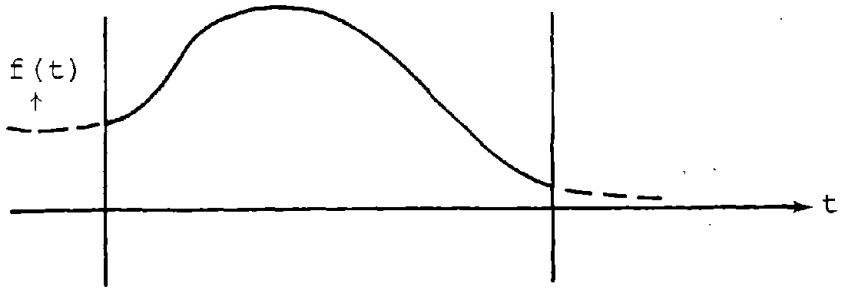

Figure 20. Finite Interval of a Function of Time

Within this interval there are still infinitely many data points, and the computer has a finite number of words in which to store data points, usually on the order of several thousand to several tens of thousands. Therefore, it is necessary to sample f(t) within this interval:

Figure 21. Samples of Time Interval in Figure 20

Obviously, information is lost in reducing f(t) to samples with an interval. However, the event producing the occupant motion sensor signal is usually quite short, on the order of 100 msec or less. If we sample at a rate of 2000 samples/sec, the Sampling Theorem (6,7) indicates that we will lose frequency components in our signal (i.e., in its spectrum) above 1 kHz. This frequency is well above that of any meaningful signal from an occupant motion sensor, as discussed in Section 2.0.

At this point we should discuss the computer actually used in this project. The Honeywell DDP-516 has a core memory of

32768 16-bit words. Of this, half are used by the programs needed to perform the computation and the operating system which controls the programs. The remaining 16384 words are used to contain 8192 floating point numbers. (Each requires 2 words, or 32 bits, to give seven decimal places of accuracy.) Each complex data point requires 2 floating point numbers to hold the real and imaginary parts, so there is a maximum of 4096 data points which can be stored. The present programs are using half of this maximum, or 2048 points, so that at 2000 samples/sec the total time interval is 1.024 sec. With this amount of data, the execution of the scheme in Figure 19 requires approximately 3 min. of computer time. In the future, it will be possible to double the number of data points, if that is found necessary.

The programs used in this project have been written in FORTRAN and are run under the Disc Operating System which is standard on this computer. The FFT subroutine, named FORT, was adapted from the program of the same name supplied by the I.B.M. SHARE library. A Hewlett-Packard 7200A Graphic Plotter is attached to the computer and is used to draw time functions or their spectra in standard and quickly understood graphic form. The occupant motion sensor data from the field tests will be recorded on magnetic tape and used as input to an analog-to-digital converter which is attached to the computer. The computer will then be able to sample the data directly, perform Fourier analysis, and digitally filter the sensor signal.

As mentioned above, the output of an occupant motion sensor will contain useful information about acceleration, velocity, etc., plus noise. The *a priori* assumption is that in the spectrum of this signal the noise will be present in the higher frequencies, while the actual phenomenon we wish to measure will occur at lower frequencies. That is, the actual occupant motion will occur more slowly than the ringing and noise. We therefore desire that our filter be some form of low-pass filter, one which passes low-frequency components of a signal while reducing or removing high-frequency components. Low-pass filters are usually described by two qualifications: a qualitative term describing the shape of $|H(\nu)|$ (the magnitude of the complex number $H(\nu)$), and the frequency ν_h at which $|H(\nu_h)| = \frac{1}{\sqrt{2}}|H(o)|$, known as the half-power point. It is so called because power is proportional to the square of a signal, and at the half-power point:

$$|H(\nu_h)|^2 = \frac{1}{2}|H(o)|.) \qquad (21)$$

Within this definition, one can propose a variety of such filters. Those evaluated in this project are shown in Figures 22-24.

These filters are defined as follows:

Sharp cutoff:

$$H(\nu) = \begin{cases} 1 & |\nu| < \nu_h \\ 0 & |\nu| > \nu_h \end{cases} \tag{22}$$

RC filter:

$$h(t) = \begin{cases} 0 & t<0 \\ e^{-t/\tau} & t\geq 0 \end{cases} \tag{23}$$

Which implies

$$H(\nu) = \frac{1}{1+i2\pi\nu\tau} \tag{24}$$

and thus, $$\tau = \frac{1}{2\pi\nu_h} \text{ so that } |H(\nu_h)| = \frac{1}{\sqrt{2}} \tag{25}$$

Amplitude - only RC filter:

$$H(\nu) = \frac{1}{\sqrt{1+(2\pi\nu\tau)^2}} \text{ where } \tau = \frac{1}{2\pi\nu_h} \tag{26}$$

Note that $|H(\nu)|$ is the same as in (23).

Gaussian filter:

$$H(\nu) = e^{-k\nu^2} \quad \text{where } k = \frac{\ln 2}{2\pi(\nu_h)^2} \tag{27}$$

This is the shape of a Gaussian or normal curve.

Martin-Graham filter:[5]

$$H(\nu) = \begin{cases} 1 & |\nu| < \nu_2 \\ 0 & |\nu| > \nu_T \\ \frac{1}{2}\left[1+\cos\frac{\pi(|\nu|-\nu_c)}{\nu_T-\nu_c}\right] & \nu_c<|\nu|<\nu_T \end{cases} \tag{28}$$

Since no actual test data were as yet available, a synthetic signal was devised to test the filters proposed above. The head acceleration curve from run No. 4882 in the Holloman report[6] (Figure 25) was chosen as an example of the type of

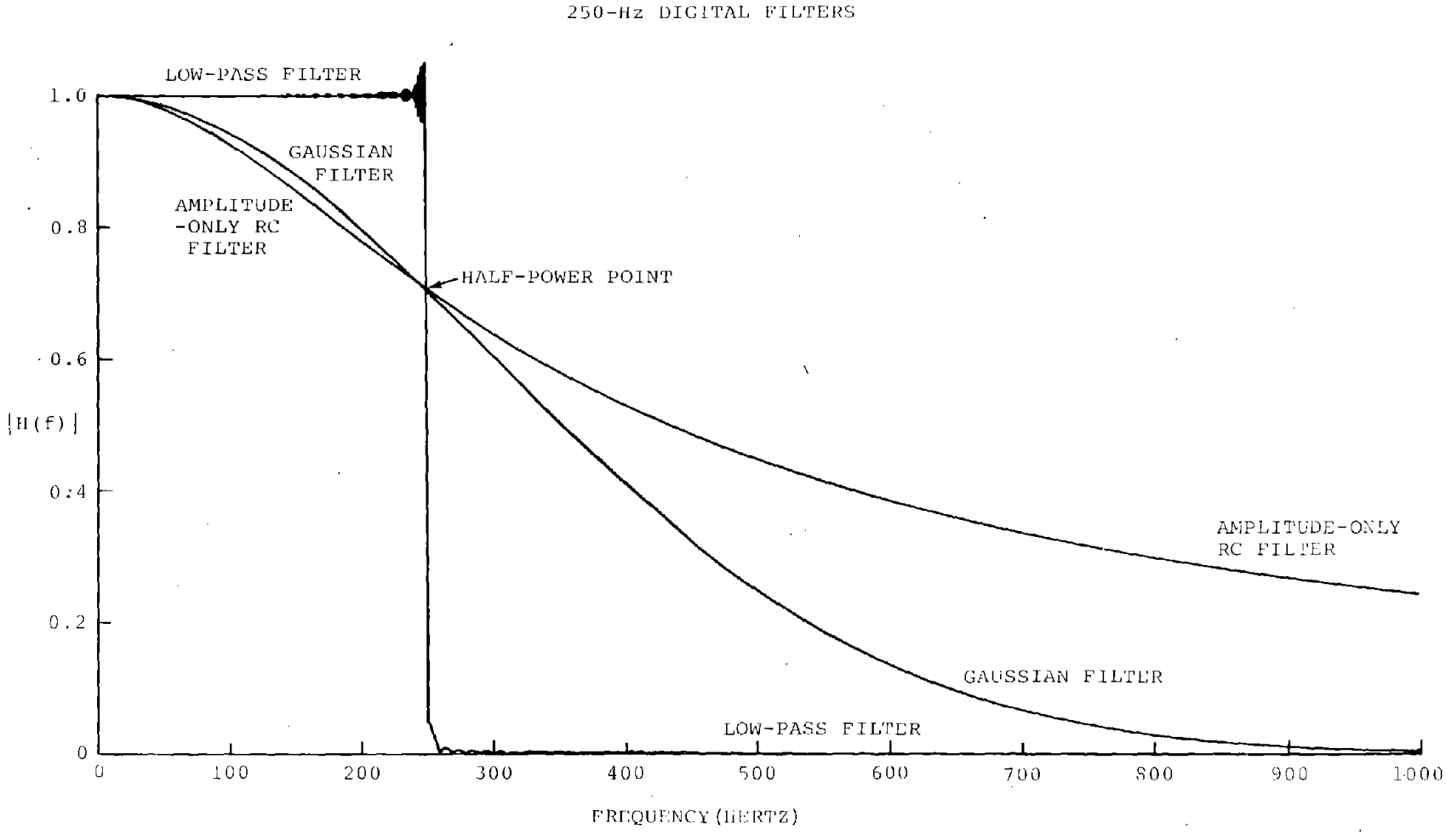

Figure 22. 250-Hz Digital Filters

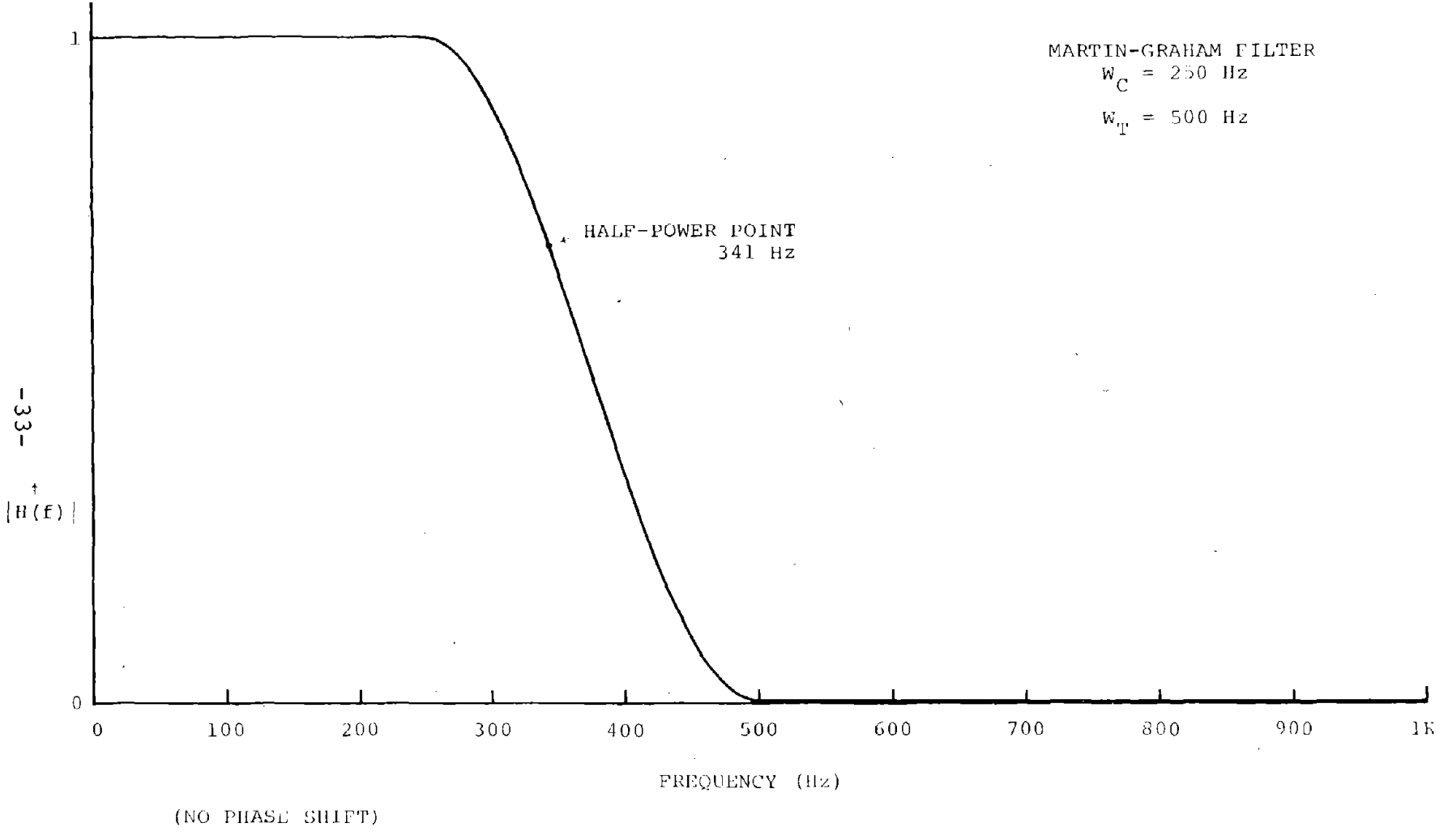

Figure 23. Martin-Graham Filter

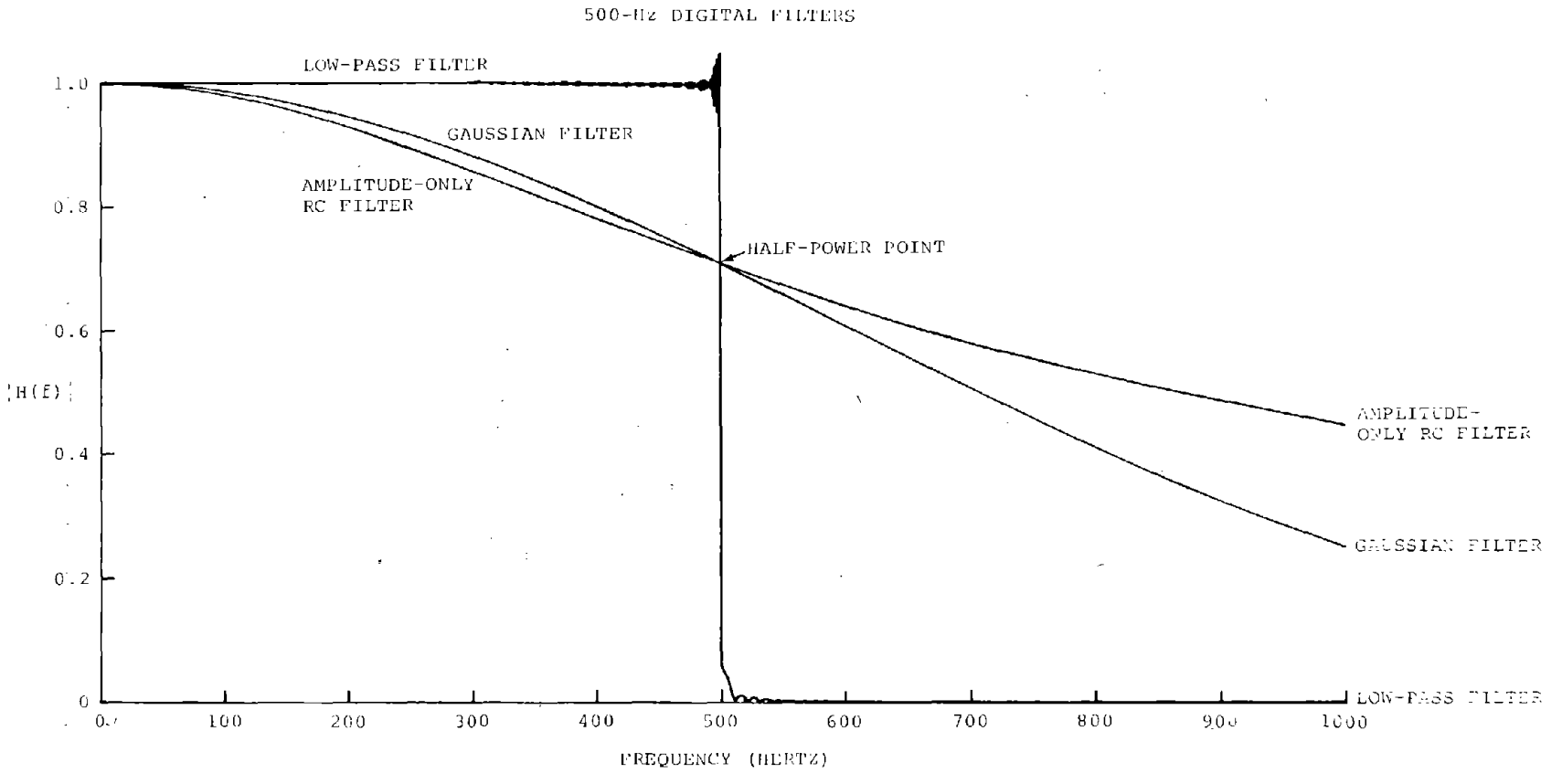

Figure 24. 500-Hz Digital Filters

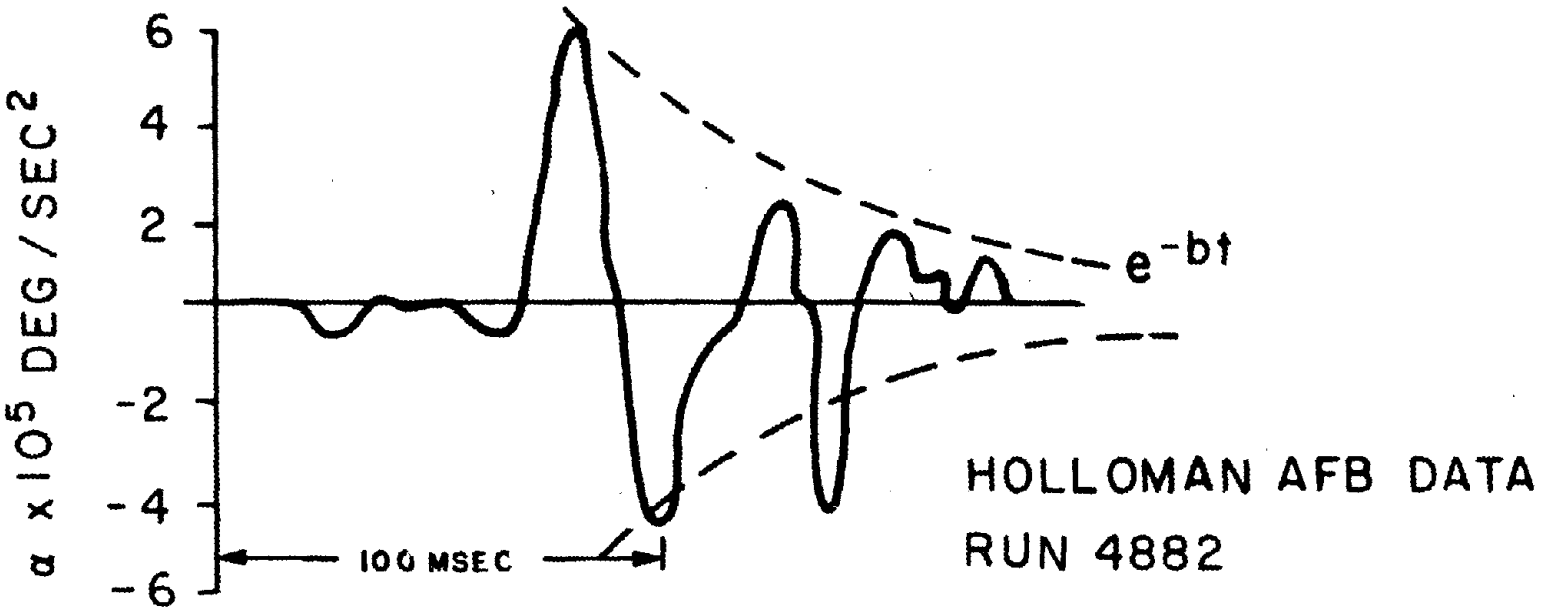

Figure 25. Example of Signal from Sensor

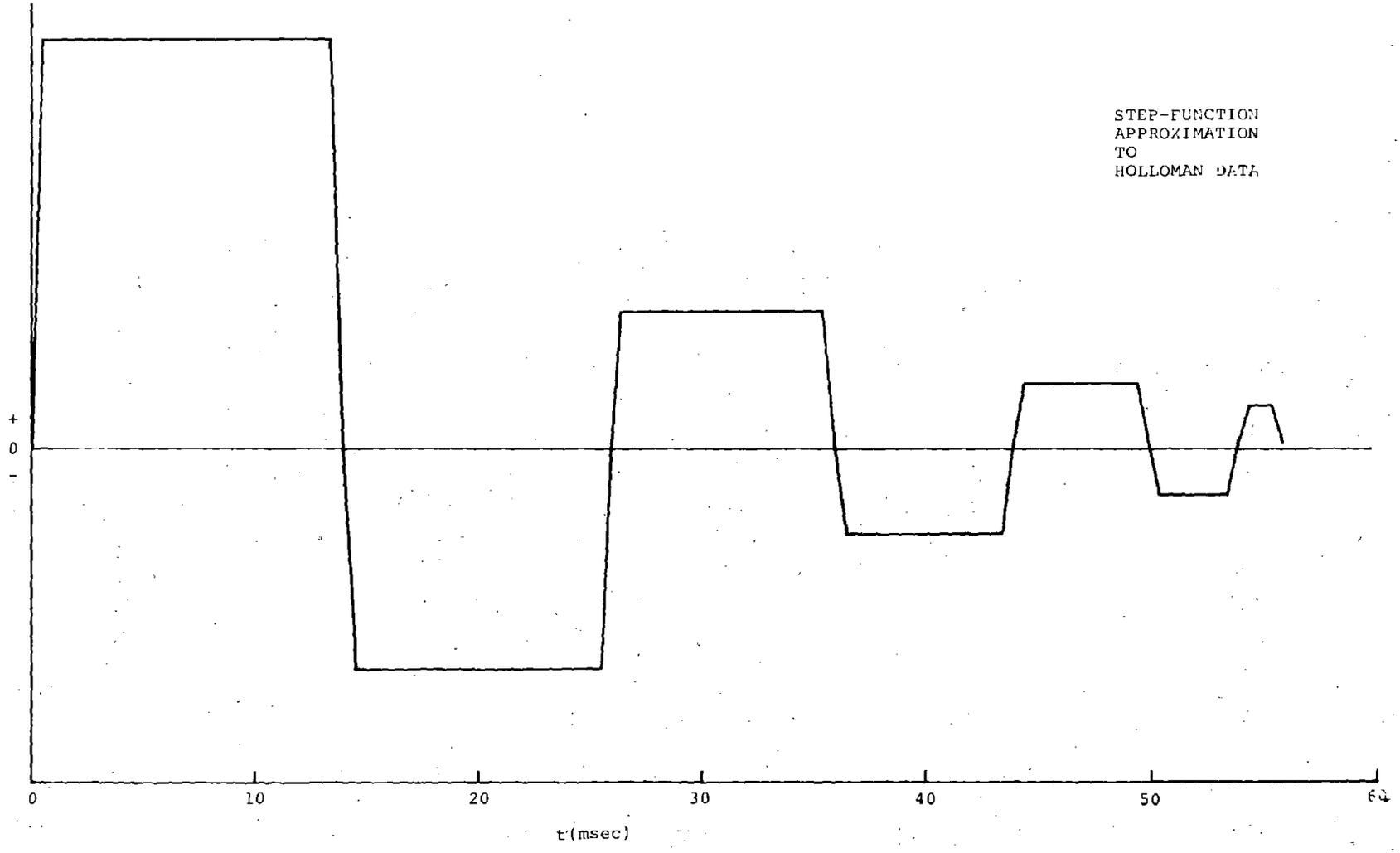

Figure 26. Squared-off Approximation to Figure 25

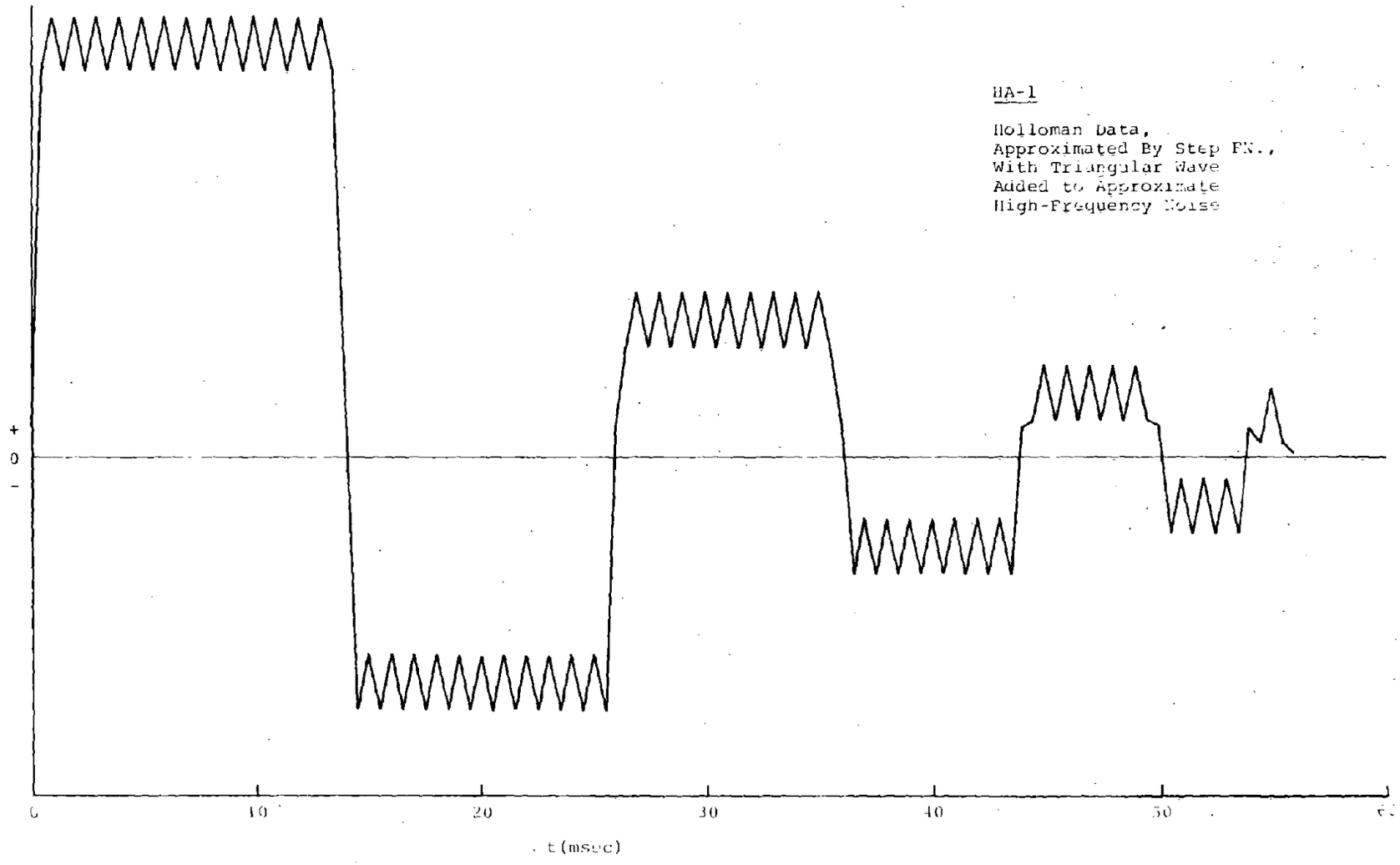

Figure 27. Figure 26, With Added Noise

signal to be expected. Unfortunately, it had already been filtered at 100 Hz, so our synthetic signal was squared off to add higher frequency components. (See Figure 26). To simulate high-frequency noise, a constant value was alternately added to and subtracted from successive sample points of this signal. (See Figure 27.) This was the synthetic signal used to test filters. The object was to remove the noise and recover the signal of Figure 26 with minimum distortion. The outputs of the various filters tested are shown in Figures 28-32. All the filters had ν_h = 250 Hz, except for the Martin-Graham filter, which had ν_h = 341 Hz for ν_C = 250 Hz, ν_T = 500 Hz. Note that the sharp-cutoff and Martin-Graham filters remove the noise but remove too many desired frequency components and distort the signal causing spurious ringing. Both RC filters have less distortion but remove only about 80% of the noise. The Gaussian filter is obviously best of all. Note in Figure 32 that it passes more intermediate frequencies than the sharp-cutoff or Martin-Graham filters, and that it rolls off more steeply to remove high-frequency noise better than the RC filters.

This conclusion shows another advantage of digital filtering. If we attempt to process a signal with a real, physical filter, we are restricted to those filters for which $h(t) = 0$ for $t < 0$, known as realizable filters. This occurs because no real stable physical system can have an output before it receives any input. A digital filter only exists as a set of complex numbers, and need not be electronically or physically realizable. In the examples above, only the real RC filter is realizable. The Gaussian filter, which we see to be superior in this case, has $h(t)$ in the shape of a normal curve, and is non-zero for all t.

There is one point where care should be taken in this procedure. The input signal may contain a sharp peak which may be considerably reduced by the filter. Since the Safety Standards are set up to rule on peak values of acceleration, force, etc., the type of filter used could conceivably determine whether a particular restraint system passes or fails. Therefore, care must be taken by comparing data before and after processing as described in this section.

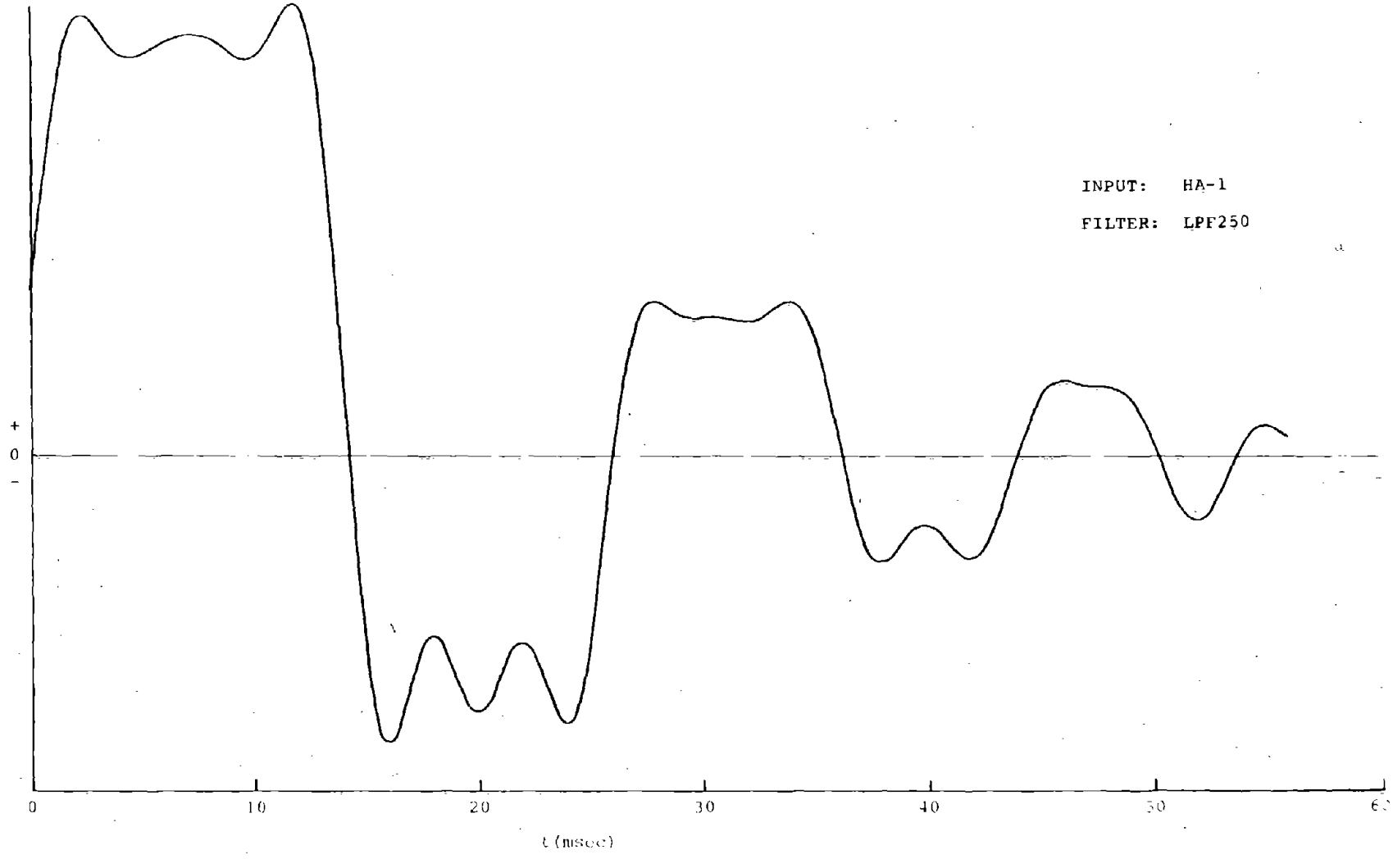

Figure 28. Result of Filtering with 250-Hz Sharp-Cutoff Filter

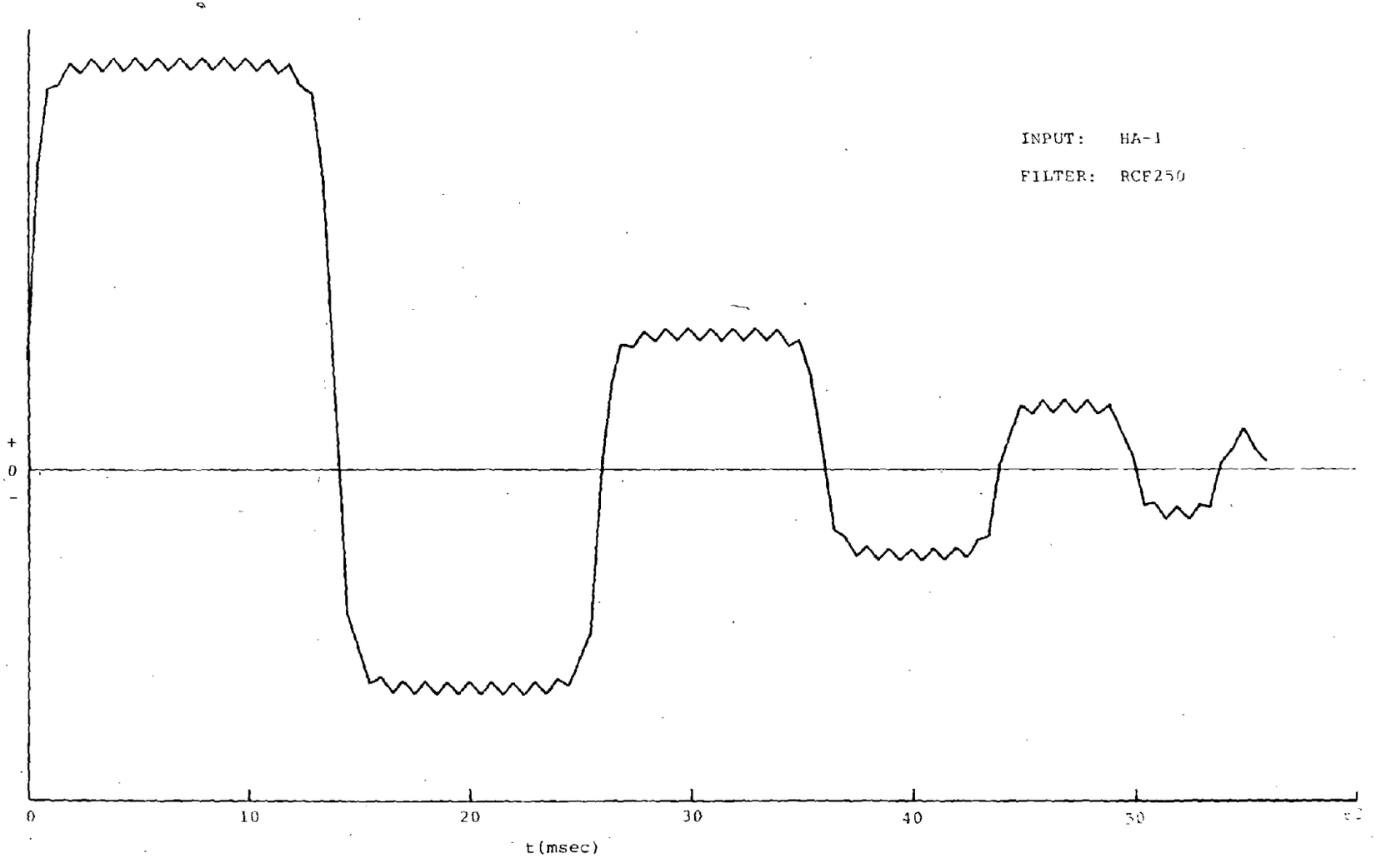

Figure 29. Result of Filtering with 250-Hz Amplitude-Only RC Filter

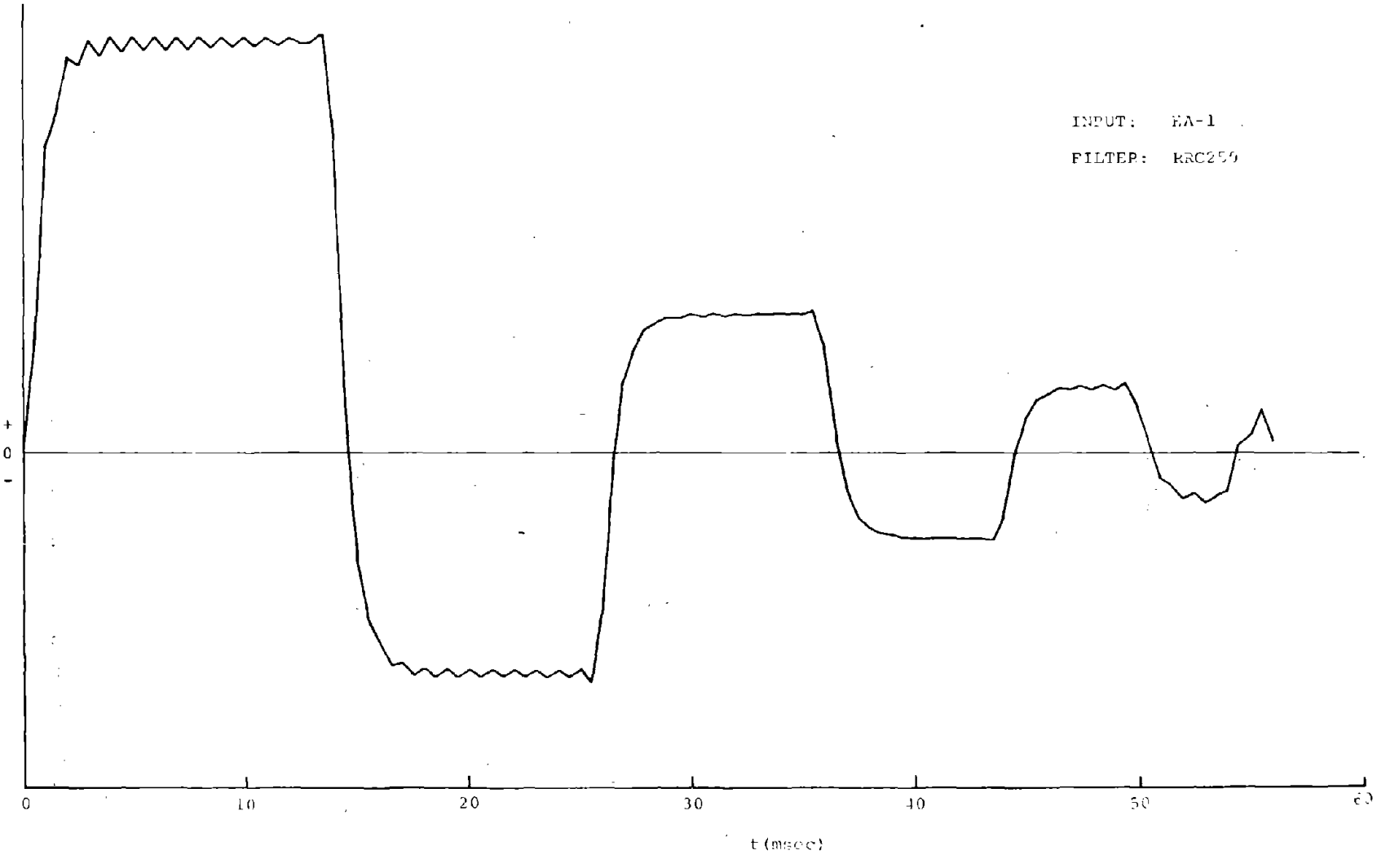

Figure 30. Result of Filtering with 250-Hz RC Filter

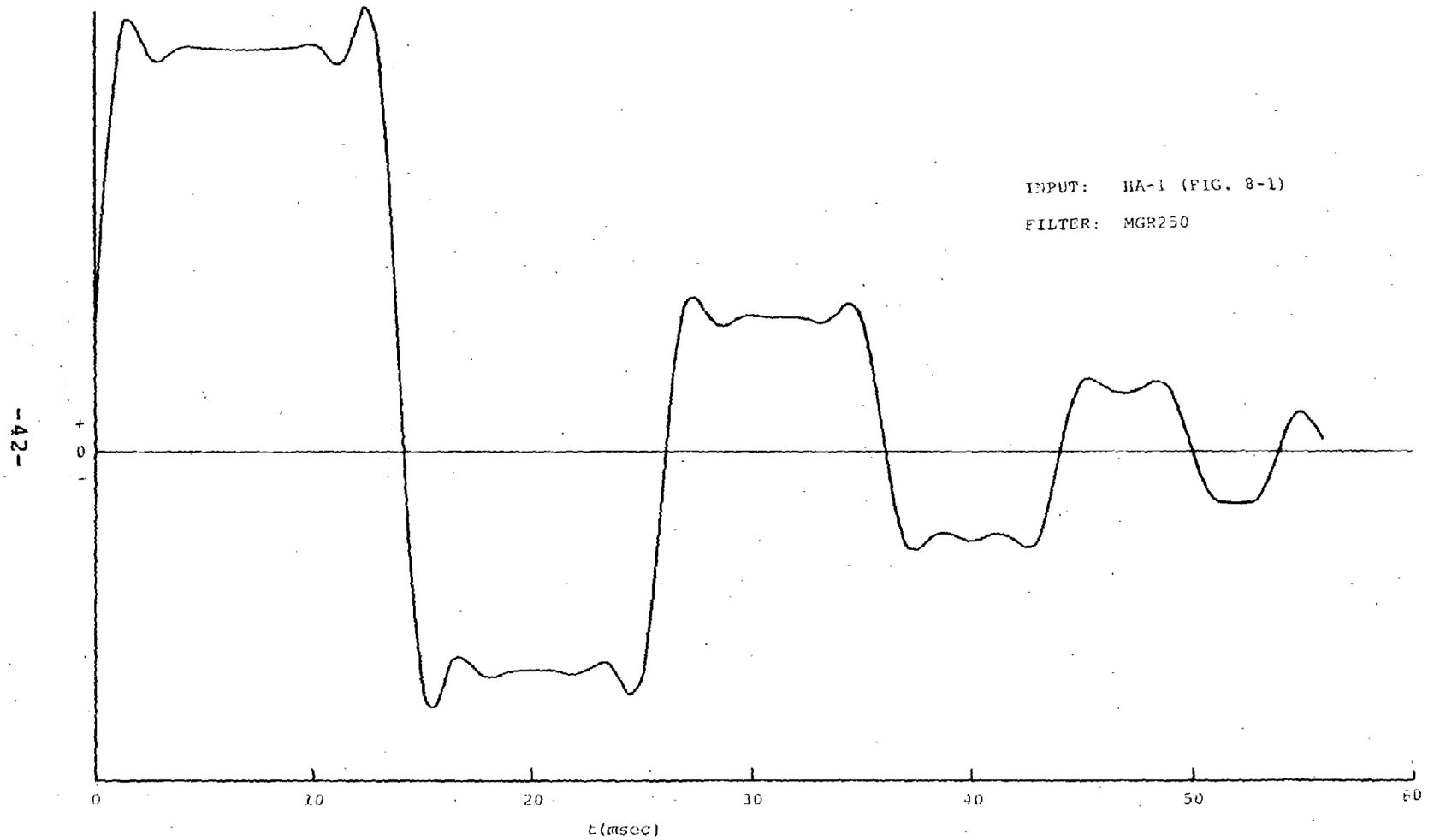

Figure 31. Result of Filtering with Martin-Graham Filter; ν_c = 250 Hz, ν_T = 500 Hz

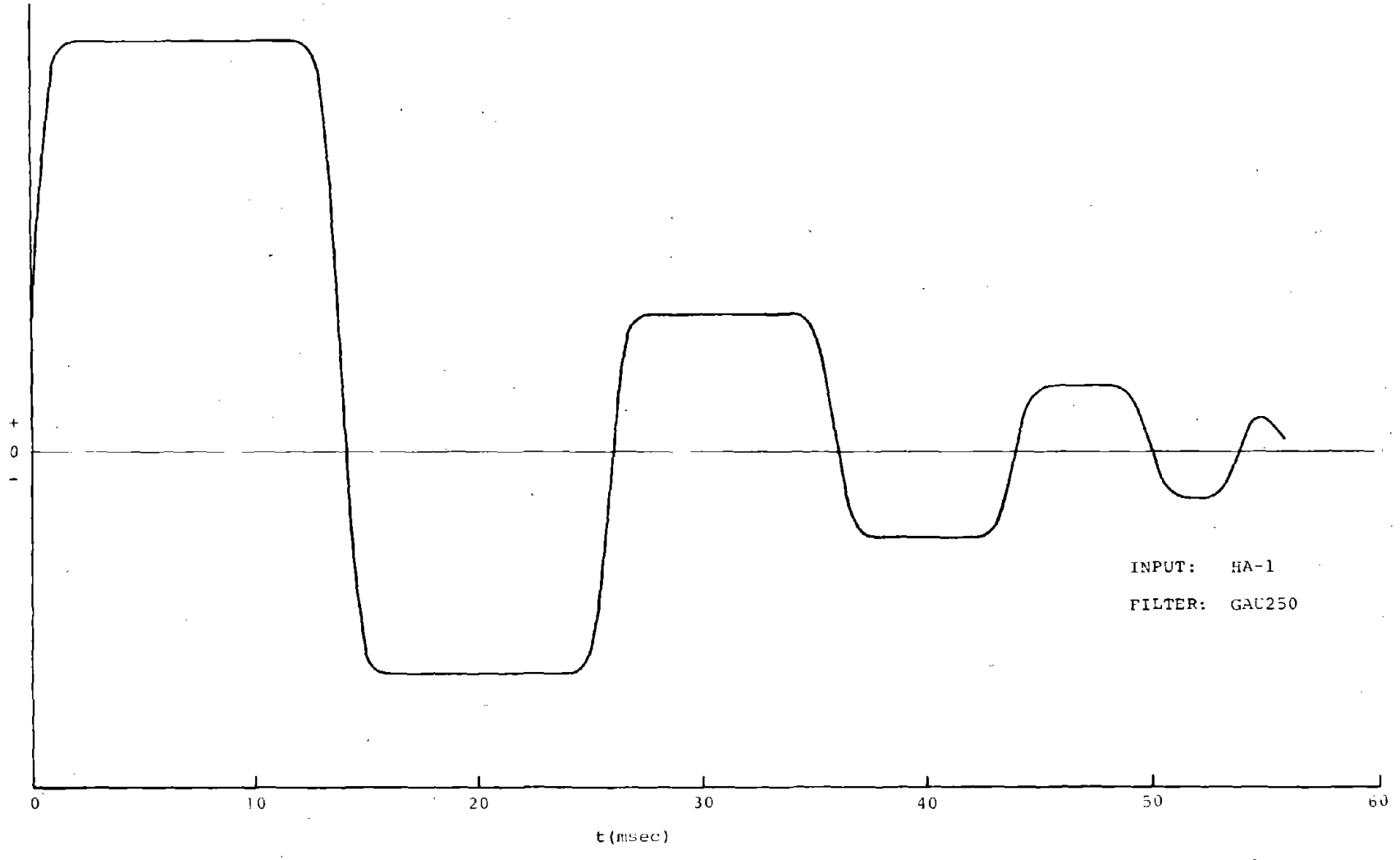

Figure 32. Result of Filtering with 250-Hz Gaussian Filter

4.2 ERROR INTRODUCED BY DIFFERENTIATION OF A NOISY SIGNAL

We often find that we have raw data from an experiment in the form of the position of an object as a function of time. An example is the sequence of pictures from a high-speed camera which records a deceleration experiment. Usually we are more interested in velocity or acceleration, so it is necessary to differentiate the data. This derivative can be approximated at any point by taking the data at a point t and a point separated from it by Δt:

$$\frac{dx}{dt} = \frac{x(t+\Delta t) - x(t)}{\Delta t} \qquad (29)$$

However, the data may be noisy, and this noise may be amplified by this differentiation. A computer simulation was performed as follows:

A sensor signal with known derivative was assumed and set up as a sequence of data points. To each data point, a noise signal was added. The following assumptions were made about the noise encountered in this type of experiment:

1. It adds to the signal.
2. It has zero mean, known standard deviation, σ, and a normal (Gaussian) distribution.
3. Its value at any point is independent of its value at any other point.

These noise values were generated by a power-residue method for generating random numbers in the computer. One noise value was derived from the average of a sum of twelve random numbers so generated. By the Central Limit Theorem from probability theory such a set of values will have the properties listed above.

The data points, now consisting of signal plus noise, were differentiated using equation (29). The error of this procedure is taken to be σ, the standard deviation of the differentiated noisy signal. The relation of the error in the differentiated signal to that in the original signal is shown in Figure 33.

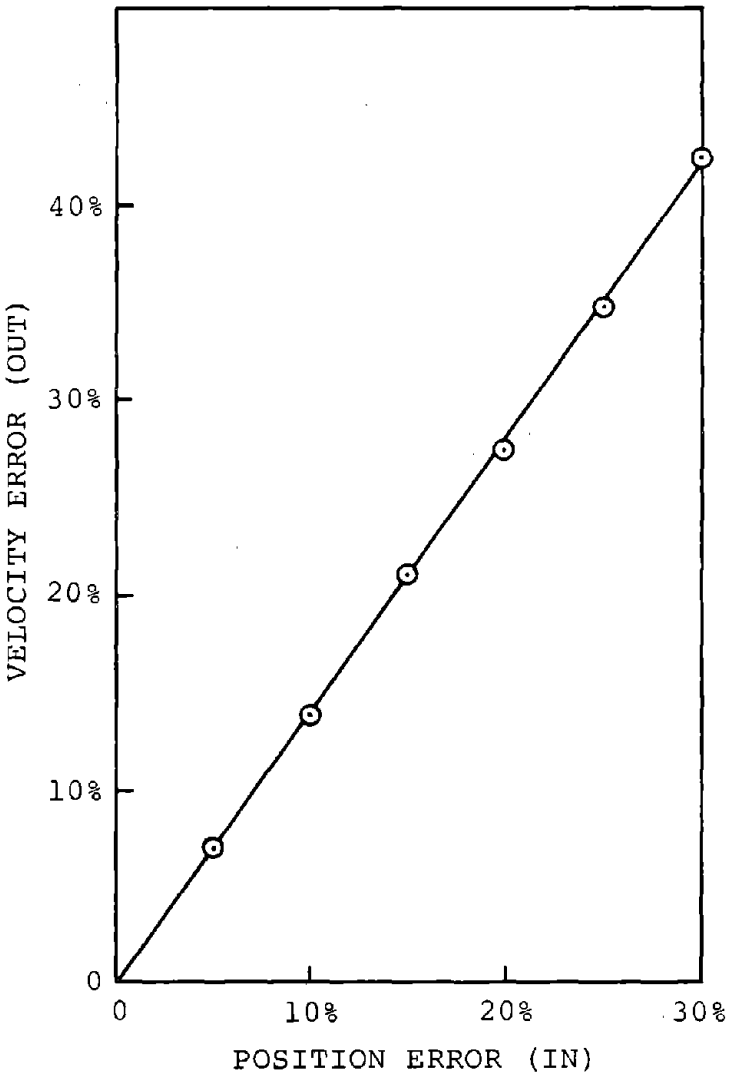

Figure 33. Error Increase by Differentiation

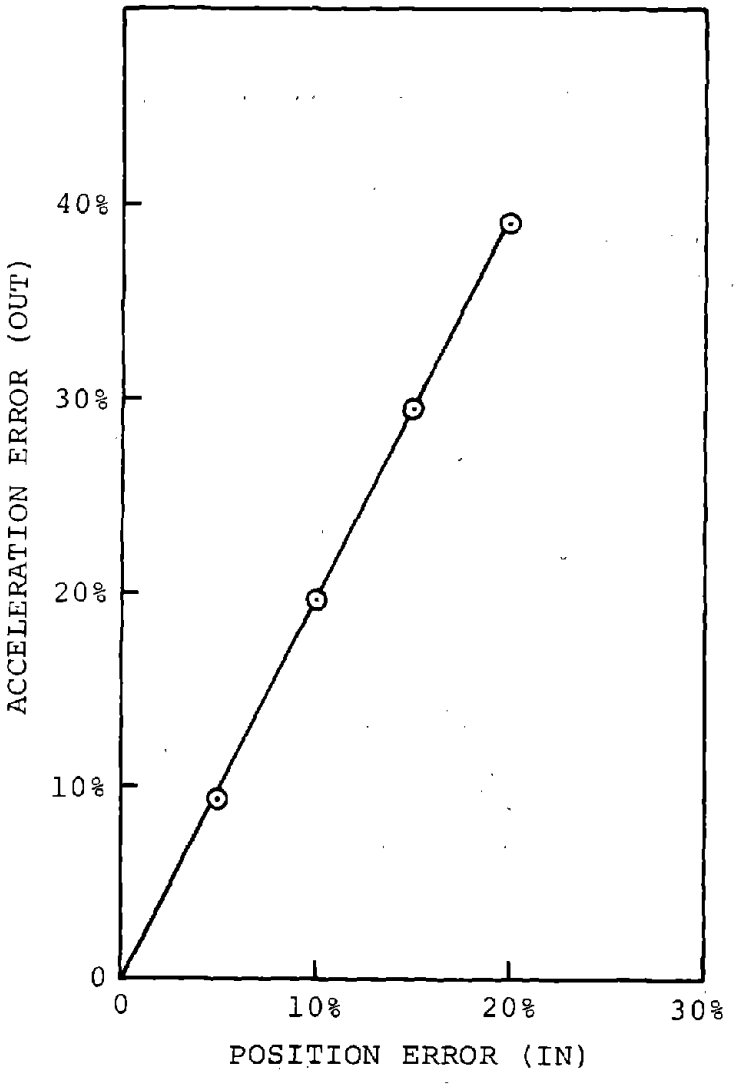

Figure 34. Error Increase by Double Differentiation

If we apply these results to the double differentiation of a camera positional signal (to obtain acceleration), we find the error approximately double for small values and getting progressively worse for large initial errors. This is shown in Figure 34. The conclusion of this for occupant motion sensing is that if one requires good acceleration or velocity data from a high-speed camera record of a sled test, one must obtain a very good original film recording of the event.

5.0 FIELD TESTING

Field testing of several of the systems described in this report will be performed at deceleration test facilities, including the following:

Liberty Mutual Research Center
Hopkinton, Mass.

Holloman Air Force Base

Johnsonville Naval Air Development Center

Cornell Aeronautical Laboratory
Buffalo, N.Y.

These systems have been combined into a portable package which can be set up at ongoing tests at the above facilities and which does not interfere with existing equipment. The basic package is shown in Figure 35. It includes on-board electronics, a 150-foot 28-conductor cable, a patch panel and calibration unit, signal conditioning electronics, and a 12-channel FM tape recorder. It can be moved in a station wagon.

Field testing began during the latter part of FY71 at the Liberty Mutual Research Center, with the static APD tests described in Section 3.5.5. The test set-up is illustrated in Figure 36. Dynamic tests on the various candidate sensors will follow. Future testing at the other locations in FY72 will begin tests with live subjects; this will allow evaluation of the scheme for mounting instruments on a bite bar.

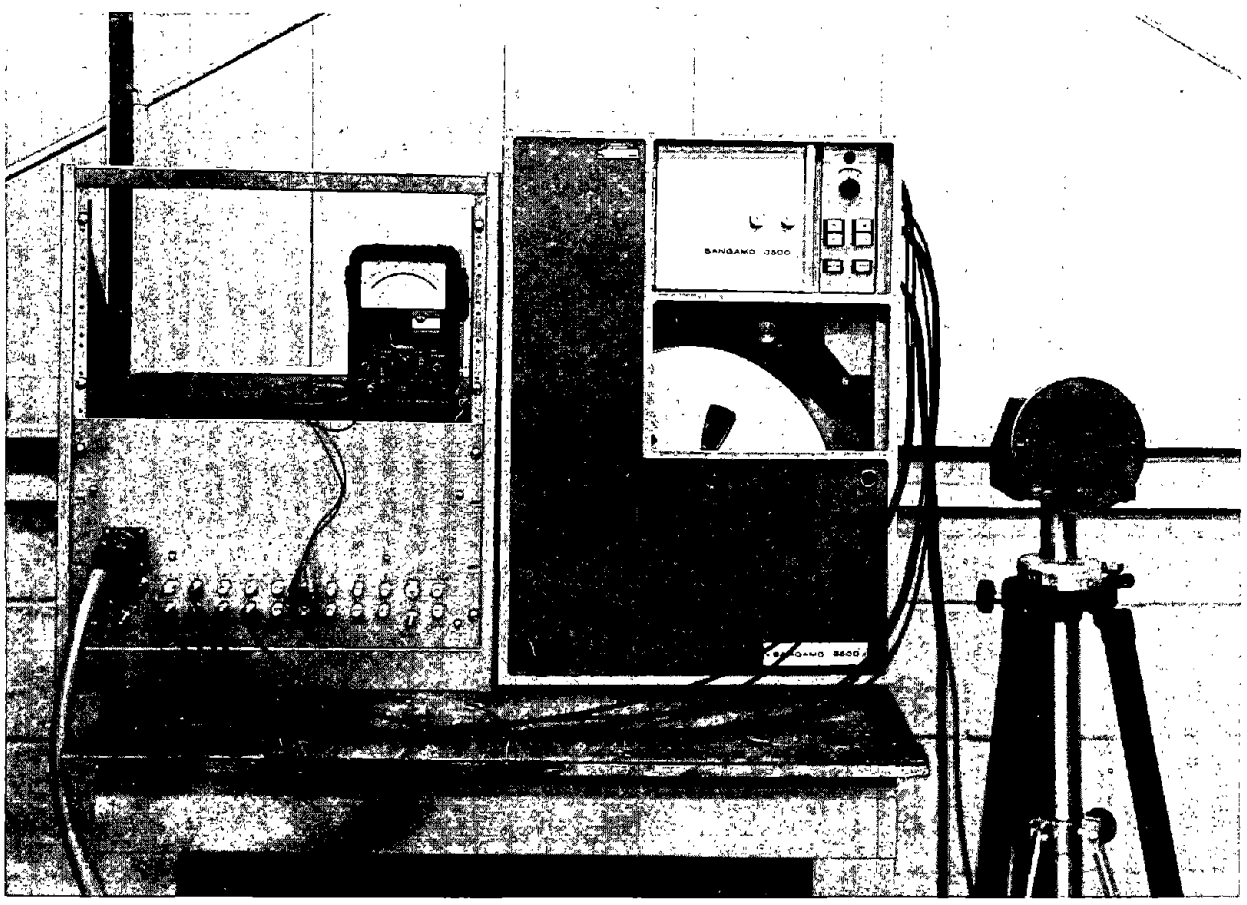

Figure 35. Basic Test Package

Left: Patch panel with umbilical cable to sled.
Right: Data recorder.
Far Right: Reference field coil for APD system.

Figure 36. APD Mounting for Static Tests

Deceleration sled. Seated anthropometric dummy is wearing the APD head sensor. Foreground: on-board impedance converters and patch panel chassis, with umbilical cable connected.

APPENDIX A

GENERAL SPECIFICATIONS

For purposes of establishing a uniform coordinate system to allow a systematic analysis of the measurement problem, a hip, upper torso, and head model is used. The hips are allowed one degree of translational movement. The upper torso is allowed one degree translation and one degree rotation within the sagittal plane. The head is allowed three degrees rotation and two degrees of translation in the sagital plane. This model can readily be expanded to include additional degrees of freedom. However, this simple model does take into consideration neck extension and compression, neck twist relative to the torso, and torso acceleration. For simplicity the back is considered a rigid member. The coordinate system is shown below in Figure A-1.

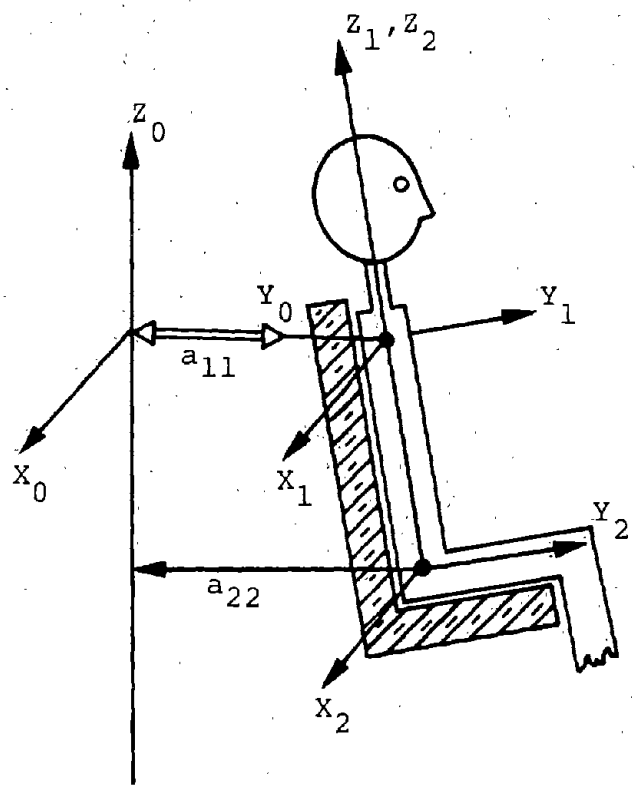

Figure A-1. Coordinate system

Below is a list of desired body motion measurements, together with the importance or priority of each (rated 1 to 3 - high to low) and the maximum value expected for each.

	Maximum Value	Priority
Head Rotations		
ϕ	+120°, -180°	
$\dot{\phi}$ *	10^4 deg/sec	
$\ddot{\phi}$ **	10^6 deg/sec^2	
(Measured around x_1 Axis)		1
Head-Neck Extension or Compression		
$(z_1 - z_2)$	$\pm$ 5 cm	
$(\dot{z}_1 - \dot{z}_2)$	1 meter/sec	
$(\ddot{z}_1 - \ddot{z}_2)$	10^3 meter/sec (100 g's)	1
θ_A	$\pm$ 90°	
$\dot{\theta}_A$	10^2 deg/sec	
$\ddot{\theta}_A$	10^4 deg/sec^2	
(Measured around y_1 Axis)		2
θ_B	$\pm$ 90°	
$\dot{\theta}_B$	10^2 deg/sec	
$\ddot{\theta}_B$	10^4 deg/sec	
(Measured around z_1 Axis)		2
Rotation of Shoulder Chest		
(Center of $x_1y_1z_1$ System)	$\dot{\beta}$ = 10^4 deg/sec $\ddot{\beta}$ = 10^6 deg/sec^2	3

* A single dot indicates a velocity (d/dt)
** A double dot indicates acceleration (d^2/dt^2)

Translation of Hips

(Center of $x_2y_2z_2$

System)

$\dot{y}_2$	20 meters/sec	
$\ddot{y}_2$	10^3 meters/sec^2 (100 g's)	3

A fixed coordinate system, $x_oy_oz_o$, is also shown in Figure A-1. It is the reference system against which all other measurements will be made. It will either be the frame of the sled or crash vehicle, or an earth based system. The choice will be determined by the types of transducers finally selected. The motions of a_{11} and a_{22} will allow one to convert measurements in the $x_1y_1z_1$ or $x_2y_2z_2$ system to the absolute $x_oy_oz_o$ system.

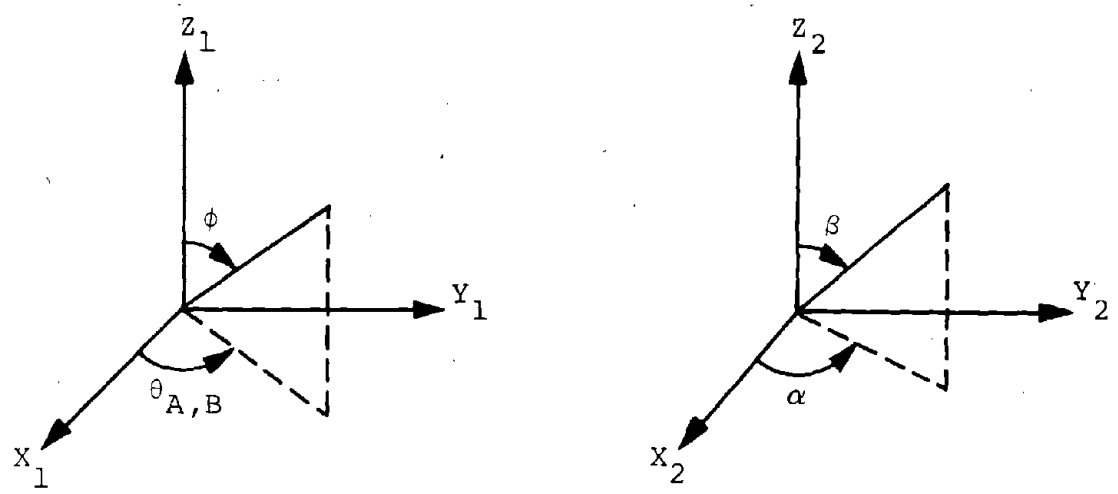

Figure A-2. Fixed Coordinate System

MEASUREMENT PRECISION

Absolute - 10%

Trial to Trial - 5% Repeatability

CALIBRATION

Laboratory calibration traceable to NBS standards.

Field calibration - limited sensor self-calibration; complete electronic field calibration before and after test; validation tests, comparison with accelerometer and photo data from non-air-bag dummy tests.

APPENDIX B

SKIN MOTION STUDIES

If a sensor is attached to the skin of a subject, the fact that the skin is loosely attached to the body and can move with respect to the body will create an error. One would expect this error to increase with the mass of the sensor, which exerts an inertial force on the skin during a deceleration event. The following curves show the relative motion of the skin of the forehead under a shear-type, tangential, force:

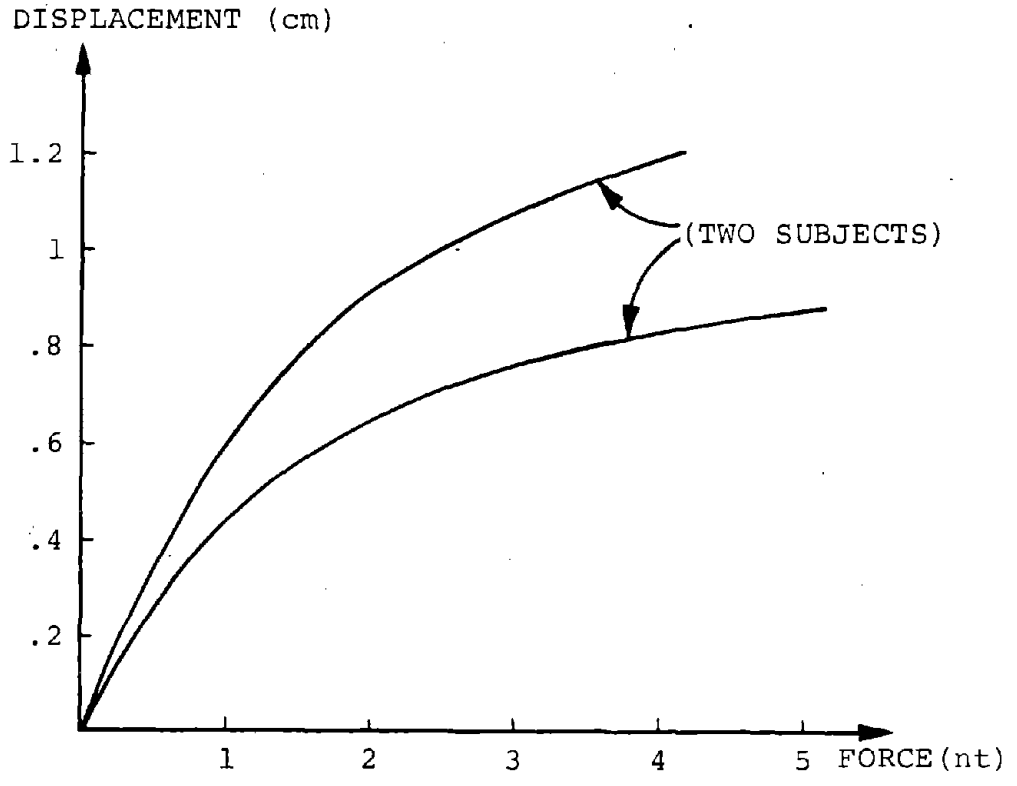

Figure B-1. Skin Displacement vs Force

Consider the example of measurement of forward head acceleration in the sagittal plane. We are given:

$$\ddot{\phi} \leq 10^6 \text{ deg/sec}^2 \qquad \text{(B-1)}$$

$$\dot{\phi} \leq 10^4 \text{ deg/sec} \qquad \text{(B-2)}$$

For maximum $\ddot{\phi}$, we can find how long it takes for $\dot{\phi}$ to reach its maximum:

$$\dot{\phi} = \ddot{\phi} t \qquad \text{(B-3)}$$

Putting in maximum values, $t = 10^{-2}$ sec. In this time, ϕ increases by:

$$\phi = \frac{1}{2} \ddot{\phi} t^2 \qquad \text{(B-4)}$$

Again using maximum values and t as solved for above, ϕ = 50 deg = 0.87 radians. If the radius of rotation is 10cm, the sensor moves through a distance of:

$$d = \phi r = (0.87) \cdot (10\text{cm}) = 8.7\text{cm} \qquad \text{(B-5)}$$

If we are to have less than 5% error, the force the sensor exerts on the skin must not move the skin more than 5% of d, or .43 cm. From this, the above curves imply a maximum force of less than one newton (nt). In this experiment, the maximum $\ddot{\phi}$ is 10^6 deg/sec^2, or approximately 17450 rad/sec^2, implying a maximum tangential acceleration at the skin of $\ddot{\phi}r$ = 1745 m/sec^2. For a sensor of mass m:

$$F_{max} = ma_{max} = m(1745 \text{ m/sec}^2) \leq 1 \text{ nt} = 1 \text{ kg-m/sec}^2 \qquad \text{(B-6)}$$

This implies:

$$m \leq \frac{1}{1745} \text{ kg} = 0.57 \text{ grams}$$

Thus a sensor attached to the skin must have a mass less than one gram, which is very small. This argues for attaching the sensor to some more fixed point, such as a bite bar.

BIBLIOGRAPHY

1. Anders, E.B., Spikes, P.W., Lasaine, A.D., Taylor, J.T., Johnson, J.J., Digital Filters, NASA CR-136.

2. Clarke, T.D., Department of Transportation, Daisy Track Balloon Lethal Tolerance Tests, Final Report, June 1970.

3. Cooley, J.W. and Tukey, J.W., An Algorithm for the Machine Computation of Complex Fourier Series, Mathematics of Computation, 19, 297-301, April, 1965.

4. Gold, B. and Rader, C.M., Digital Processing of Signals, McGraw-Hill, 1969.

5. Horner, J.L., Occupant Motion Sensors Interim Technical Report, No. DOT-TSC-NHSB - 71-1, March 1971.

6. Mason and Zimmerman, Elec. Signals and Systems, Wiley.

7. Siebert, W.M., Notes for 6.05-6.053 Signals and Systems, (Preliminary Edition, February 1965), Massachusetts Institute of Technology, 1965.